SYSTEMATIC FEATURES IN THE STRUCTURAL CHEMISTRY OF THE URANIUM HALIDES, OXYHALIDES AND RELATED TRANSITION METAL AND LANTHANIDE HALIDES

J.C. TAYLOR

Chemical Technology Division, AAEC Research Establishment, Private Mail Bag, Sutherland 2232, N.S.W. (Australia)

CONTENTS

A. INTRODUCTION

The general chemistry of the actinide halides and oxyhalides, including structural aspects, has been reviewed up to the end of 1971 by Brown [1—3], Bagnall [4,5] and Keller [6]. A survey of the structural chemistry of actinide fluoride complexes by Penneman et al. [7], and a general article by Moseley [8] on the structural chemistry of lanthanide and actinide compounds takes the literature up to the end of 1972. Since that time, however, there has been much definitive new work, including a systematic study of the uranium halides and oxyhalides by neutron powder profile analysis at the AAEC Research Establishment, Lucas Heights. Structures precisely determined at Lucas Heights with this powerful technique include UCl$_3$ [9], UBr$_3$ [10], UI$_3$ [11], UCl$_4$ [12], UOCl$_2$ [13], UCl$_6$ [14] and β-WCl$_6$ [15], UO$_2$Cl$_2$ [16], UO$_2$Cl$_2 \cdot$ D$_2$O [17], UF$_6$ [18—20] and the homologues MoF$_6$ [21,22] and WF$_6$ [23,24]. A precise study of UF$_6$ has been made by single-crystal neutron diffraction [20].

The new types UBr$_4$ [25,26] and UOF$_4$ [27—30] have been confirmed by structural analysis. More polymorphic varieties have been found, including β-UCl$_5$ [31], β-ThCl$_4$ [32], β-ThBr$_4$ [33], β-UOF$_4$ [27] and further examples in the transuranium trihalides (see Sect. D). New divalent transuranium structures have been determined by Baybarz [34,35]. While working at Lucas Heights, we found incorrect structural interpretations and diagrams (e.g. a 9-coordinate diagram for UF$_3$) in the review literature, and there were doubts about the coordination in other compounds because of lack of, or inadequate, illustration (e.g. U$_2$F$_9$). These incongruities are, hopefully, removed here. When existing diagrams have been thought to be inadequate or misleading, they have been redrawn.

Another review of certain aspects of uranium structural chemistry is timely

but, because of the size of the field, discussion is confined to the halides, oxy-halides and related compounds. Illustrations and Tables have been chosen as the best media to describe the systematic features of the structures. In its documentation, this work owes a great deal to the earlier systematisation used by Brown [1—3].

(i) Polyhedral arrangements of anions around uranium

The bonding in these compounds is largely ionic and, to a first approximation, the crystal structures may be considered as an assemblage of positive uranyl or uranium cations and negative anions. As to the shape of the anion polyhedra around uranium, polyhedral packing, anion bridging, minimisation of repulsive effects and the atomic sizes themselves influence the shape as well as directional effects from the bonding orbitals. Thus, polyhedral shapes cannot be predicted from the theory of covalent bonding alone.

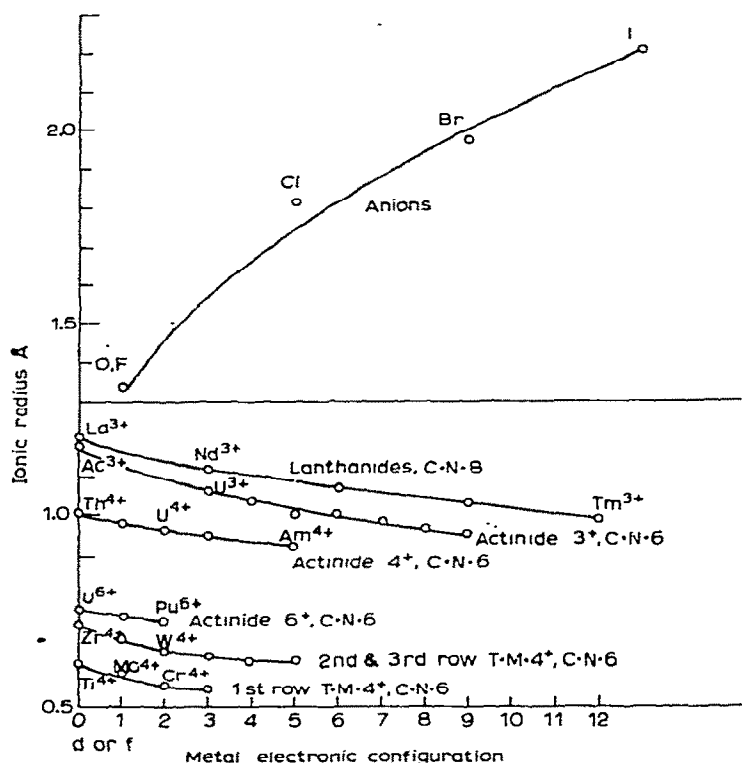Size effects [36] are obvious from Fig. 1. The actinides and lanthanides are

Fig. 1. Ionic radii of some actinide, lanthanide and transition metal ions, compared with the radii of the oxygen and halogen anions (data from Shannon and Prewitt [36]).

large cations, more capable of supporting a larger number of anions around them than the second and third row d-transition metal ions. Since the trivalent lanthanide and actinide ions are about the same size, it is not surprising to find structure types common to both series. For a given cation, the coordination number (C.N.) drops in the order F, Cl, Br, I, because of the anion size. The chemistry of uranium is interesting because of its oxidation state range of 3—6. There is a great size difference in going from U^{3+} to U^{6+} (Fig. 1) and this causes the C.N. to increase from 6 in UF_6 to 11 in UF_3. The size range in both the U cation and the anions results in a large number of polyhedral types being found around uranium in these compounds. On the other hand, the structural chemistry of the transition metal halides lacks this variety, the C.N. almost invariably being 6, except for the larger Zr^{4+} and Hf^{4+} ions.

Calculations based on bonding theory or minimisation of repulsive energies with some form of inverse power law are of no predictive value in these systems because the polyhedra for C.N. 7 and above differ so little in shape. However, the old radius ratio concept [37] gives some correlation between polyhedron type and ionic size, and is useful as a rough guide. Recently, Smith [38] proposed a novel size criterion, i.e. the use of solid angles subtended by anions at the central atom. For an efficiently arranged polyhedron, there should be few "windows", and the total solid angle subtended by the anions should approach 4π, or

$$S = \sum_n 2\pi \left(1 - \cos\left(\sin^{-1} \frac{r}{L}\right)\right)/4\pi$$

should approach 1 (r is the van der Waals' radius and L the bond length). Families of halides have similar S values. Thus, uranyl compounds, where the uranyl group is linear, have low S values, whereas compounds with extensive bridging have S values near 1. The efficiencies of different polyhedra with the same C.N. can be checked by calculating S values. Smith also introduced a convenient notation for polyhedra, e.g. 4.4. for a cube, 4/4 for a square antiprism, 1.5.1 for a pentagonal bipyramid, 1.4/4.1 for a bicapped square antiprism and so on. For a detailed study of the solid angle approach we must await Smith's full paper.

According to Kitaigorodskii [39], a first-rate theory predicts, a second-rate theory forbids and a third-rate theory provides a post-factum "explanation". On this count, the radius ratio and solid angle theories fall short, as well as theories using molecular orbital or valence bond theory only, or repulsive minimisation only, in predicting high C.N. polyhedra. For a proper solution, a problem must be properly defined and then the variables determined, perhaps with a least-squares process with a large ratio of observations to variables. At present the polyhedron problem has not been fully defined. King [40] has tabulated orders of stability based on the degrees of repulsion exhibited in various polyhedra.

TABLE 1

The 5f actinide, 4f lanthanide and 3d—5d transition metal series in the periodic system

Series	Group								
	3a	4a	5a	6a	7a		8		1b
(a) Transition metal series									
3d	Sc	Ti	V	Cr	Mn	Fe	Co.	Ni	Cu
4d	Y	Zr	Nb	Mo	Tc	Ru	Rh	Pd	Ag
5d	(4f) La—Lu	Hf	Ta	W	Re	Os	Ir	Pt	Au
(b) Actinide series									
Actinide (5f)	Ac	Th	Pa	U	Np	Pu	Am	Cm	Bk···
Actinide valence	3	4	4,5	3—6	3—7	3—7	2—6	3,4	3,4

(ii) The position of uranium in the periodic system

The region around Pa and U in the periodic system is crucial, being near a "crossover" point in the binding energy versus atomic number curve [41] for the 5f and 6d electrons; this makes it difficult to predict theoretically which orbitals are being used in any covalent bond formation. The 5f actinide series is analogous to the 4f lanthanide series and, lower down, to the d-transition series (see Table 1). The d-transition analogues, Mo and W, have a chemistry similar in some respects to that of uranium in a corresponding valence state. The transition metal analogues of uranium are Cr, Mo and W.

(iii) Polyhedra around uranium in the halide and oxyhalide compounds

The numerous alkali halide—actinide fluoride complexes are mentioned only in passing as they have been considered by Penneman et al. [7]. Some idealised polyhedra for C.N. from 6 to 14 are given in Fig. 2. Many of these are found in the uranium compounds reviewed here; some observed polyhedra for the uranium halides and oxyhalides are shown in Figs. 3 and 4. Some size trends may be seen (e.g. increasing C.N. with reduction of metal oxidation number and constant anion; increasing C.N. with constant cation and reducing anion size) and there is a wide variety of polyhedra.

Of special interest are UF_3 and U_2F_9, whose structures are quite difficult to illustrate because of the extensive fluorine bridging and high C.N. values. The description of the UF_3 polyhedron was omitted in structure papers on this compound (see Sect. B(i)), and the U_2F_9 polyhedron was not discussed in the original Zachariasen paper [42] or in the subsequent neutron study (see

C.N.	Polyhedral types
6	Octahedron, Trigonal prism, Pentagonal prism
7	Pentagonal Bipyramid, Capped Octahed., Tet. Base, Trig. Base, Capped Trig. prism
8	Square antiprism, Cube, Dodeca-hedron, Bicapped octahedron, Bicapped trig. prism, Hexagonal bipyramid
9	Tricapped trig. prism, Capped Sq. anti., Capped cube
10	Bicapped Sq. anti.
11	Capped pentag. anti., Fully-capped trig. prism
12	Icosahedron, 4-Capped cube
14	Bicapped Hex. anti., Fully-capped cube

Fig. 2. Some theoretical high C.N. polyhedra.

Sect. B(iii)). Consequently, descriptions of the two polyhedra are absent from recent reviews, and an incorrect C.N. for UF_3 of 9 has been perpetuated in the review literature. One review [7] gives the polyhedron of U_2F_9 correctly as a tricapped trigonal prism, but there is a question mark in the Table where it is listed (this polyhedron is a logical assumption as all other nonacoordinate fluoride complexes contain the tricapped trigonal prism).

In the oxyhalides, UO_2F_2 has a high C.N. of 8 (for valence 6) imposed on it by the linear uranyl group; $UOCl_2$ is especially interesting bécausé it contains uranium atoms in 7-, 8-, and 9-coordination in the one structure. The polyhedra in these compounds are generally distorted from the ideal shapes by bridging requirements and repulsive effects. Plates 1—10 in the review by
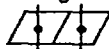
Uranium binary halides

U Valence	F	Cl	Br	I
6	UF_6 — Octahedron	UCl_6 — Octahedron	—	—
5	α-UF_5 Octahedra, β-UF_5 Penta. bipy.	UCl_5 Octahedral dimer	—	—
4,5	U_2F_9 — Tricap-trigonal prism(TCTP)	—	—	—
4	UF_4 Square antiprism	UCl_4 Dodecahedron	UBr_4 Pentagonal bipyramid	—
3	UF_3 Fully capped trigonal prism	UCl_3 Tricapped trigonal prism	UBr_3 Tricapped trigonal prism	UI_3 Bicapped trigonal prism

Fig. 3. Observed anion polyhedra in the uranium binary halides.

Muetterties and Wright [43] show very clearly the small differences in ideal polyhedra with the same C.N. Thus, it is not surprising to find the polyhedron in ThI_4 described as both square antiprismatic and dodecahedral in that review. A good way to check the polyhedron type would be to calculate least-squares χ^2 values, fitting the observed polyhedron to various ideal ones and then choosing the one having the lowest χ^2 residual. This, however, has not been done in any of the papers surveyed here.

(iv) Isostructural series and polymorphism

There are many possible compounds in the halides and oxyhalides of the actinides, lanthanides and transition metals; over 70 actinide binary halides, 60 actinide oxyhalides and 70 binary transition metal fluorides are known. Fortunately, the structural chemistry of these compounds is simplified by the occurrence of isostructural series based on "structure types". The abundance of isostructural types may be made possible by the predominance of size and packing factors over spatial differences in the bonding orbitals in the various series. Table 2 shows the isostructural series which occur in the actinides, and

TABLE 2

Actinide halide isostructural series

	Ac	Th	Pa	U	Np	Pu	Am	Cm	Bk	Cf	Es
MCl_2							$EuCl_2$				
MBr_2							$EuBr_2$			$EuBr_2$	
MI_2		'ThI$_2$'					EuI_2				
MF_3	UF_3			UF_3	UF_3	UF_3	UF_3	UF_3	UF_3 YF_3	UF_3 YF_3	UCl_3
MCl_3	UCl_3			UCl_3	UCl_3	UCl_3	UCl_3	UCl_3	UCl_3	UCl_3	
MBr_3	UCl_3			UCl_3	UCl_3 UI_3	UI_3	UI_3	UI_3	UI_3 $FeCl_3$ $AlCl_3$	UI_3 $FeCl_3$ $AlCl_3$	
MI_3		'ThI$_3$'	UI_3	UI_3	UI_3	UI_3	UI_3 $FeCl_3$	$FeCl_3$	$FeCl_3$	$FeCl_3$	
MF_4		UF_4	UF_4	UF_4	UF_4	UF_4	UF_4	UF_4	UF_4	UF_4	
MCl_4		α-ThCl$_4$ UCl_4	UCl_4	UCl_4	UCl_4						
MBr_4		α-ThBr$_4$ UCl_4	UCl_4	UBr_4	UBr_4						
MI_4		ThI_4		UI_4							
M_2F_9			U_2F_9	U_2F_9							
MF_5			β-UF$_5$	α-UF$_5$ β-UF$_5$							
MCl_5			$PaCl_5$	α-UCl$_5$ β-UCl$_5$							
MBr_5			UBr_5 β-PaBr$_5$	UBr_5							
MI_5			PaI_5								
MF_6				UF_6	UF_6	UF_6					
MCl_6				UCl_6							

Uranium oxyhalides

	F	Cl	Br
U Valence	UO_2F_2 Fused hexagonal bipyramids $UO_2F_{6/3}$	UO_2Cl_2 Pentagonal bipyramid $UOO_{/2}Cl_{4/2}O_{/2}$	$[UO_2Br_2]$
6	α-UOF_4 Pentagonal bipyramids $UF_2OF_{4/2}$ β-UOF_4 Pentagonal bipyramids $UF_2OF_{4/2}$	$UO_2Cl_2 \cdot D_2O$ Pentagonal bipyramid $UO_2Cl_{4/2} \cdot OD_2$	
5	(U_2OF_8) (UO_2F)	(UO_2Cl) $UOCl_3$ Fused pentagonal bipyramids $UO_{3/3}Cl_2Cl_{2/2}$	(UO_2Br) $UOBr_3^-$ $UOCl_3$ type
4		$UOCl_2$ Dodeca-hedron Tricapped trigonal prism Octa-hedron+1	$UOBr_2^-$ $UOCl_2$ type
3		$UOCl$ Monocapped square antiprism	

Fig. 4. Observed anion polyhedra in some uranium oxyhalides.

Table 3 shows the distribution of the uranium halide structural types among the transition metal and lanthanide compounds. In Table 4, the distribution of the uranium oxyhalide structure types over the same systems is given. For reasons described below, there are not many analogues in the transition metal series.

The influence of the well known actinide and lanthanide contractions can be seen in the gradation of structural types across a row. On going from left to right, the cation becoming smaller, transitions occur to polyhedra of lower C.N. Examples of this are the change from the UCl_3 to the UI_3 type at Np in the actinide tribromides, and at Gd in the lanthanide trichlorides. Where dimorphism occurs, (or even trimorphism, in the case of $BkBr_3$, see Sect. D(iii)), the high-temperature form is usually the more open structure, i.e. the one with the lower C.N. The polymorphic series are more extensive in the lower valence states where the cationic size is larger, the binding more ionic and covalency effects less important. The energy differences between alternative

TABLE 3

Distribution of U halide structure types

Structure type	C.N.	Actinides	Transition metals	Lanthanides
UF_3	11	AcF_3, UF_3—BkF_3		LaF_3—NdF_3, SmF_3, EuF_3, HoF_3, TmF_3
UCl_3	9	$AcCl_3$, UCl_3—$CfCl_3$, $AcBr_3$, UBr_3, $NpBr_3$		$LaCl_3$—$GdCl_3$, $LaBr_3$—$PrBr_3$
UI_3	8	$CfCl_3$, $NpBr_3$—$BkBr_3$, PaI_3—AmI_3		$TbCl_3$, $NdBr_3$—$EuBr_3$, LaI_3—NdI_3
UF_4	8	ThF_4—CfF_4	α-ZrF_4, HfF_4	CeF_4, PrF_4, TbF_4
UCl_4	8	$ThCl_4$—$NpCl_4$, $ThBr_4$, $PaBr_4$		
UBr_4	7	$NpBr_4$		
U_2F_9	9	Pa_2F_9		
α-UF_5	6		BiF_5	
β-UF_5	7	PaF_5		
UCl_5	6	β-$PaBr_5$		
UBr_5		α-$PaBr_5$		
UF_6	6	NpF_6, PuF_6	MoF_6—RhF_6, WF_6—PtF_6	
UCl_6	6		β-WCl_6	

TABLE 4

Distribution of the uranium oxyhalide structure types

Structure type	C.N.	Actinides	Lanthanides
UOCl	9	AcOBr, PuOBr, BkOBr, CfOBr, AcOCl, NpOCl—EsOCl NpOI, PuOI, BkOI, CfOI	LaOCl—ErOCl, LaSF, CeSF, LaOBr—LuOBr, YOBr, LaSBr, CeSBr, LuOI, PmOI, EuOI, TmOI, YbOI
$UOCl_2$	7—9	$ThOCl_2$—$NpOCl_2$	
$UOBr_3$	7	$PaOBr_3$	
UO_2Cl		PaO_2Cl	
U_2OF_8		Pa_2OF_8	
UO_2F_2	8	NpO_2F_2—AmO_2F_2	
α-UOF_4	7		
β-UOF_4	7	β-UF_5	
UO_2Cl_2	7		

polyhedra are smaller in these low valence—high C.N. systems. The structural types forming the various series and transitions between them are discussed more fully in subsequent sections.

B. THE URANIUM BINARY FLUORIDES UF_3, UF_4, U_2F_9, α-UF_5, β-UF_5 AND UF_6

The uranium binary fluorides are such an interesting and important series that they warrant a section to themselves. This requires divergence from the overall format according to the subdivisions dihalides, trihalides, tetrahalides, etc., but this scheme is resumed in Sect. C. This series, which is important to the atomic energy industry, shows systematic gradations in bridging and bond type, which correlate with changes in the physical properties of the solids.

(i) UF_3

UF_3 is one of more than thirty crystals having the LaF_3 structure type. Four structures have been proposed for this type, including the first structure determination in 1931. The real structure is a distortion of the idealised model shown in Fig. 5, in a bimolecular hexagonal cell with $a' \doteq 4$ Å and $c' \doteq 7$ Å (space group $P6_3/mmc$). This polyhedron is a fully capped trigonal prism (C.N. 11). This small cell was reported by Zachariasen [44], and this small cell structure, due to Schlyter [45], is reported in Wyckoff's Crystal Structures [46], where the (small) unit cells of 31 isostructural compounds are given.

However, subsequent workers [47—53] reported additional reflexions re-
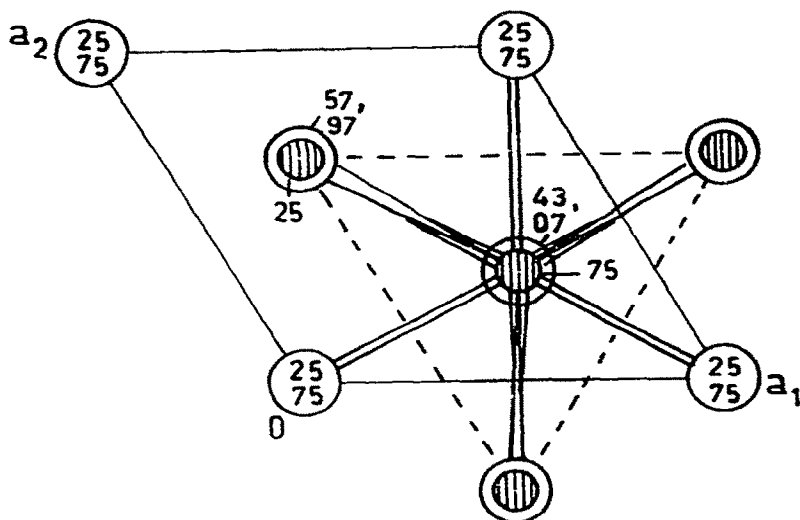
Fig. 5. The idealised, 11-coordinate, fully capped trigonal prismatic polyhedron in UF_3 (cf. ref. 45).

quiring a large unit cell with $a = a' \sqrt{3}$ and $c = c'$. The additional reflexions, with fluorine-only scattering, showed up well in the neutron studies [49,51].

Unfortunately, there is a space-group ambiguity in the big cell. Oftedal [47] proposed a structure in the space group $P6_3/mcm$, but his fluorine positions were shown to be incorrect by Zalkin et al. [48], and Laveissiere [49]. There remain the possible space groups $P6_3cm$ (hexagonal) and $P\bar{3}c1$(trigonal), which, on refinement, give slightly different distortions from the idealised structure in Fig. 5.

Zalkin et al. [48] found violations of hexagonal symmetry for LaF_3 and refined the structure in $P\bar{3}c1$. Similar coordinates for La and F were obtained by Mansmann [50]. Mansmann and Wallace [52], in a neutron powder study of the LaF_3-type HoD_3, considered the space group of HoD_3 to be $P\bar{3}c1$ also. de Rango et al. [51] carried out X-ray and neutron single-crystal and powder studies on LaF_3. Contrary to the above results, they found that hexagonal symmetry was obeyed and refined the structure in $P6_3cm$. Laveissiere [49] refined neutron powder data for UF_3 in both possible space groups and obtained the same overall R-factor (0.057) in both refinements. However, he found the "fluorine-only" reflexions gave a lower R-factor in $P6_3cm$ (0.106) than in $P\bar{3}c1$ (0.135), thus favouring the hexagonal space group. Choi [53], in a neutron diffraction study of LaF_3, also favoured the hexagonal space group.

Although the results of the above studies are conflicting, it is clear that the uranium atom in UF_3 is 11-coordinate, and not 9-coordinate,

UF₃ -P3̄c1 structure

Fig. 6. Illustration of the $P\bar{3}c1$ refinement of UF_3 neutron powder data by Laveissiere [49]. The prism fluorines are joined by dashed lines. Each prism fluorine atom is bonded to 4 uranium atoms, each of the 3 equatorial fluorines is bonded to 3 uranium atoms, and the top and bottom cap fluorine atoms are each bonded to 4 uranium atoms.

UF₃ - P6₃ cm structure
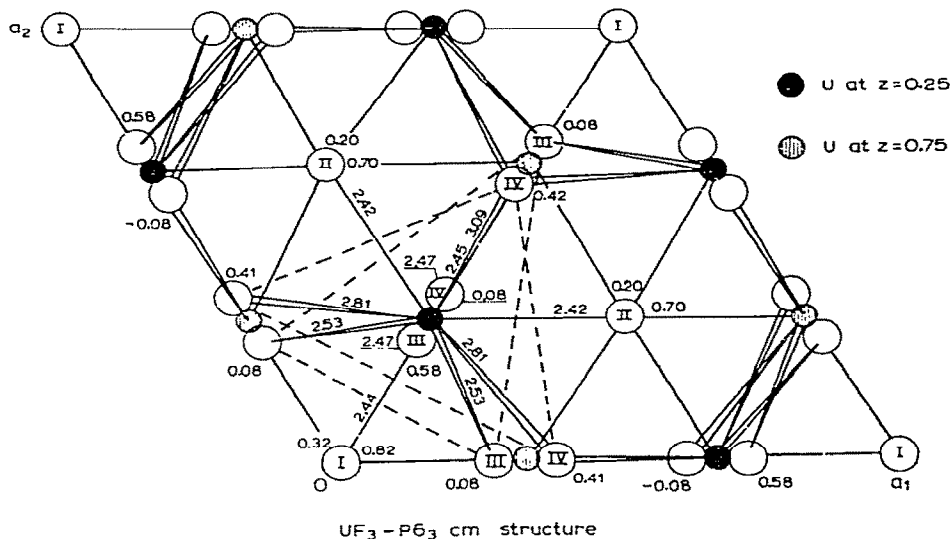
Fig. 7. Illustration of P6₃cm refinement of UF₃ neutron powder data by Laveissiere [49]. The overall bridging scheme is the same as for Fig. 6, but the fluorine positions are different for the prism fluorines. For direct comparison of the relative orientations of Figs. 6 and 7 see Sect. B(i).

whatever the space group. In recent reviews, the neutron studies [49, 51] and the 11-coordinate diagram of Mansmann [50] have been overlooked, and a 9-coordinate diagram [48] is given. The coordinates of the neutron refinements of Laveissiere in P3c1 and P6₃cm for UF₃ have been drawn in Figs. 6 and 7 (no diagrams were given in the Laveissiere paper). At first sight the alternative structures look different in the placement of the prism atoms (joined by dashed lines), but the two structures are seen to be similar when the polyhedron in Fig. 6 is rotated clockwise by 120° about [⅓, ⅓, Z] and superposed on the polyhedron in Fig. 7. The only real difference between the alternative structures is a slight relative displacement of the prism atoms, and the top and bottom cap atoms normal to c. However, there are differences in the bond lengths to the prism atoms in the two models; in P3c1 these are 3.01 (2X), 2.48 (2X) and 2.63 (2X) Å, and in P6₃cm the corresponding distances are 2.53 (2X), 2.81 (2X), 2.45 and 3.09 Å.

The finer details of the UF₃ structure are obviously still not resolved satisfactorily, but the C.N. for uranium in UF₃ is 11, and the polyhedron is a distortion of the idealised fully capped trigonal prism, originally proposed by Schlyter [45], in which the cap atoms fit firmly (bond lengths 2.42—2.48 Å), but the prismatic arrangement is distorted. Higher precision neutron diffraction studies are required to find whether Fig. 6 or Fig. 7 is correct. The uranium atoms are highly fluorine-bridged in UF₃, the bridging scheme being the same in either diagram. A possible explanation for the above anomalies could

be that some preparations crystallise in the trigonal, and others in the hexagonal space group.

(ii) UF₄

The UF₄ structure [54] is of the α-ZrF₄ type [55,46], about which there is no controversy. Since the UF₄ structure has never been well illustrated to bring out its remarkable polymeric nature, it has been redrawn in Fig. 8. Although the diagram looks complex, the structural motif is based on the use of each fluorine atom to bridge two uranium atoms. The resulting pair of independent coordination polyhedra have been described as distorted square antiprisms. A second form of UF₄ has been prepared under high-temperature and shock-wave conditions [56].

(iii) U₂F₉

Di-uranium enneafluoride (U_2F_9), was found by Zachariasen to be body-centred cubic, with $a = 8.4716(5)$ Å and space group I43m by powder X-ray diffraction [42]. The structure was confirmed by Laveissiere [57] in a powder diffraction study. This neutron diffraction study has been overlooked in all reviews of actinide structural chemistry known to the author. Neither paper contained a diagram or discussion of the polyhedron, except to say there were nine fluorine atoms around the uranium atom. The omission may be due to the difficulty in interpreting the a-axis projection, which shows the polyhedror in an unfamiliar orientation, and in a high-symmetry situation.

Wyckoff [46], Muetterties and Wright [43] and Moseley [8] did not discuss
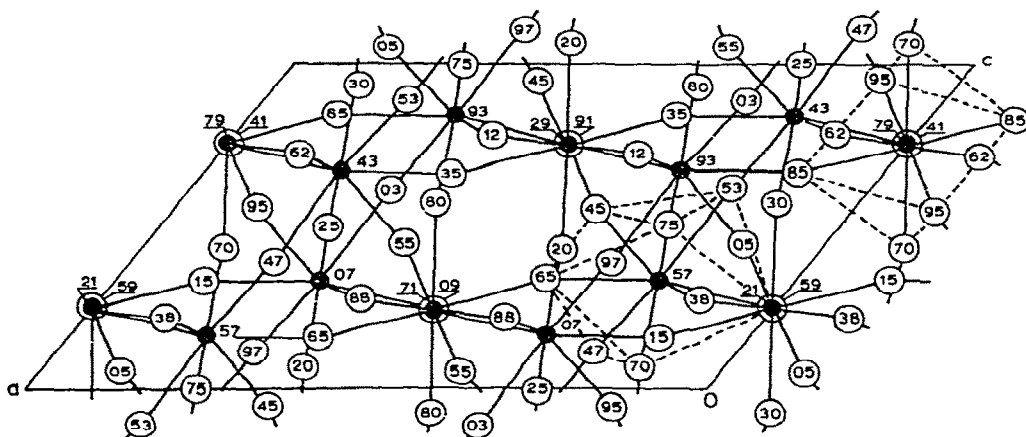
Fig. 8. The structure of UF₄ as refined by Larson et al. [54]. The two non-equivalent polyhedra, described as distorted square antiprisms [54], are shown. The heights of the atoms in hundredths of *b* are shown. Each fluorine atom bridges two uranium atoms.
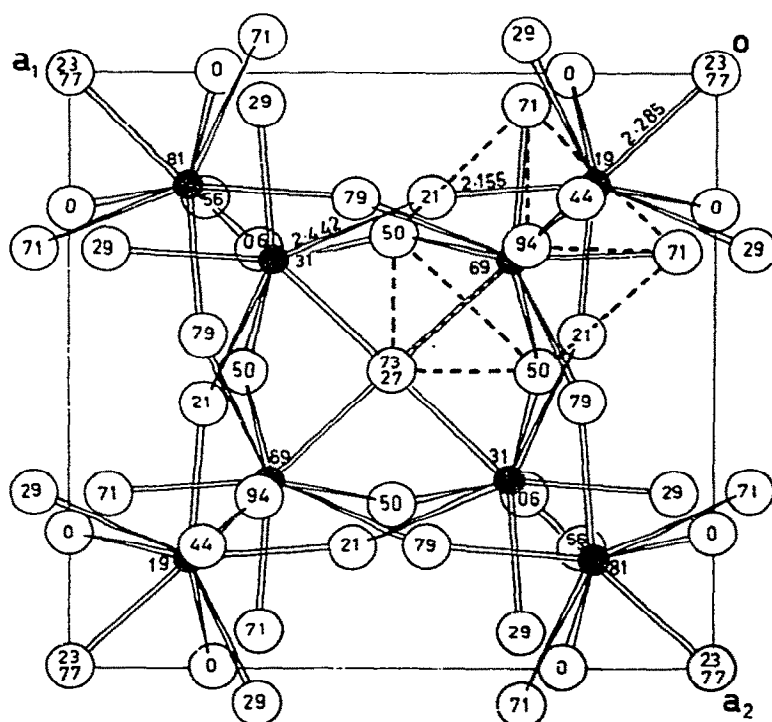
Fig. 9. The structure of U_2F_9, viewed down the cubic a_3 axis. The atomic heights are shown as hundredths of a_3. The polyhedron is outlined with dashed lines, but its type is not obvious from this projection.

the polyhedron, and Penneman et al. [7] listed U_2F_9 in their Table 6 as containing "capped trig. prism?". The a-axis projection is drawn in Fig. 9. The polyhedral type is not obvious.

When the view down [111] is drawn (Fig. 10), using the rhombohedral ($\alpha = 90°$) to hexagonal transformation, the polyhedron, viewed down the vertical 3-fold axis is immediately seen to be a symmetrically tricapped trigonal prism viewed end-on. Equivalent prisms in differing orientations around different [111] variants link corners with the first polyhedron, the prism fluorine atoms of one polyhedron becoming the capping fluorine atoms of the adjacent polyhedron, and vice versa. All the prismatic-based polyhedra are equivalent, and all corners are shared. All fluorine atoms bridge two uranium atoms. The F(1)—U—F(1) bridges are symmetrical about the $\bar{4}$ axis, with U—F(1) = 2.285(10) Å (3X) (prism) but the F(2) atoms form asymmetric bridges with U—F(2) = 2.155(10) (3X) (prism) and U—F(2) = 2.442(6) (3X) Å (cap). The longer distance is to the cap atoms. The structural formula is thus [$UF_{9/2}$].

In KU_2F_9, the coordination polyhedron is again a tricapped trigonal prism [58] with all corners shared, but in CsU_2F_9 [59] one corner is statistically
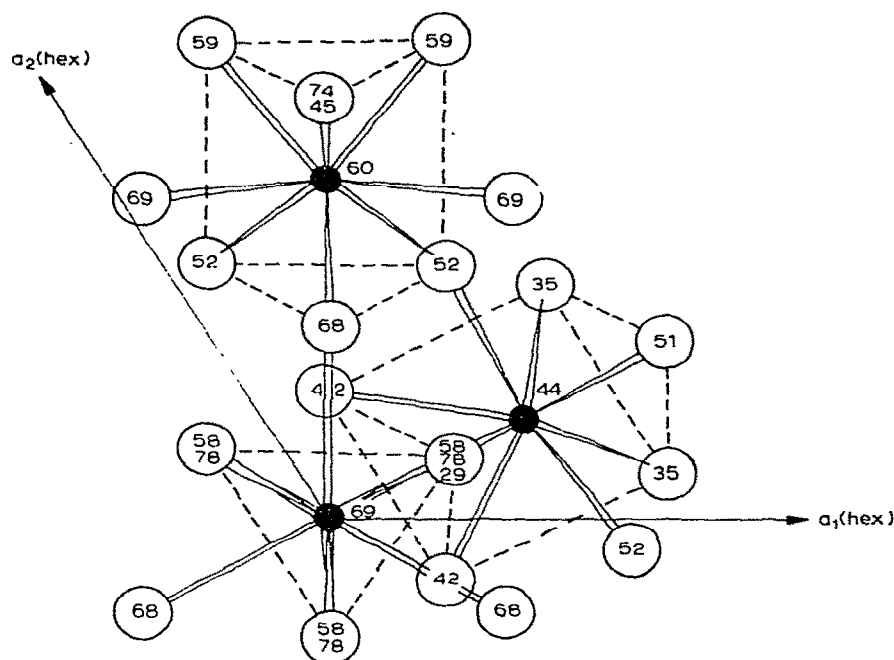
Fig. 10. The structure of U_2F_9, as seen down a [111] axis. The heights are in hundredths of the triple hexagonal cell derived from the cubic cell by the rh → hex transformation. The tricapped trigonal prisms are outlined with dashed lines.

half-occupied and unshared. In the KU_2F_9 and CsU_2F_9 papers, the structures are not compared with U_2F_9. $NaTh_2F_9$ is said to be a U_2F_9 type with the smaller sodium ions in the octahedral holes ($\frac{1}{2}$, 0,0) [42].

U_2F_9, like UF_4, is thus a highly fluorine-bridged polymer with all polyhedra corners shared. The structure is built up with tricapped trigonal prismatic polyhedra, instead of the square antiprisms which form the UF_4 structure.

(iv) α-UF₅

The α-UF_5 structure type determined by Zachariasen [60] is tetragonal, with strings of octahedra linked at opposite corners into endless chains running parallel to c (Figs. 11 and 12). BiF_5 [61] and also $WOCl_4$ and $WOBr_4$ have this structure [62], the oxygens being the bridge atoms. The C.N. is now becoming lower as a result of the reduced size of the uranium atom. This is the high temperature form of UF_5.

(v) β-UF₅

The low-temperature form, β-UF_5, also studied by Zachariasen [60], is a more condensed tetragonal arrangement of edge-shared pentagonal bipyra-

TABLE 5

Fluorine bridging schemes in UF_3, UF_4, U_2F_9, β-UF_5, α-UF_5 and UF_6

Compound	UF_3	UF_4	U_2F_9	β-UF_5	α-UF_5	UF_6
Bridging scheme	$UF_{2/4}$ (top cap), $F_{6/4}$ (prism), $F_{3/3}$ (equatorial cap)	$UF_{8/2}$	$UF_{9/2}$	$UF_3F_{4/2}$	$UF_4F_{2/2}$	UF_6
Polyhedron type	Distorted fully capped trigonal prism (C.N.11)	Distorted square antiprism (C.N.8)	Tricapped trigonal prism (C.N.9)	Pentagonal bipyramid (C.N.7)	Octahedron (C.N.6)	Octahedron (C.N.6)
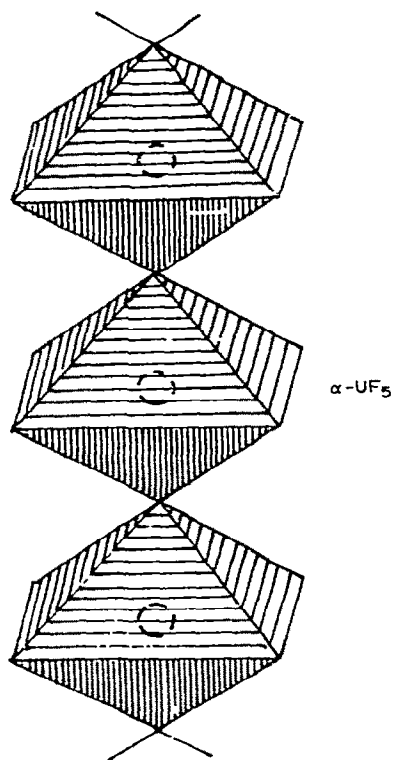
Fig. 11. The scheme of the α-UF₅ structure, showing the endless chains of *trans* corner-linked octahedra.

mids. β-UOF₄ was found to be of this type [30] with an oxygen atom replacing a fluorine atom (Fig. 13). PaF₅ also has this structure [63].

(vi) UF₆

UF₆ melts at 337.2 K, and can be kept as a solid at room temperature when encapsulated. The structure of solid UF₆ was determined by Hoard and Stroupe [64] from X-ray single-crystal data. These authors depicted the structure in terms of h.c.p. anions with uranium atoms in octahedral holes (Fig. 14). More precise fluorine positions [18,19] were determined at Lucas Heights with neutron powder studies at 193 K and 293 K. The structure was refined further in a neutron single-crystal study [20], with 475 reflexions, and gave the molecular bond lengths 1.996(4), 2.004(4) and 1.993(3) (2X) and 1.992(3) (2X). This indicated a molecular, rather than an ionic lattice. The structure of UF₆ is shown in Fig. 15, octahedra being drawn with apices at the fluorine centres. All fluorine atoms are terminal; there is no fluorine bridging. A model of the UF₆ structure is shown in Fig. 16.
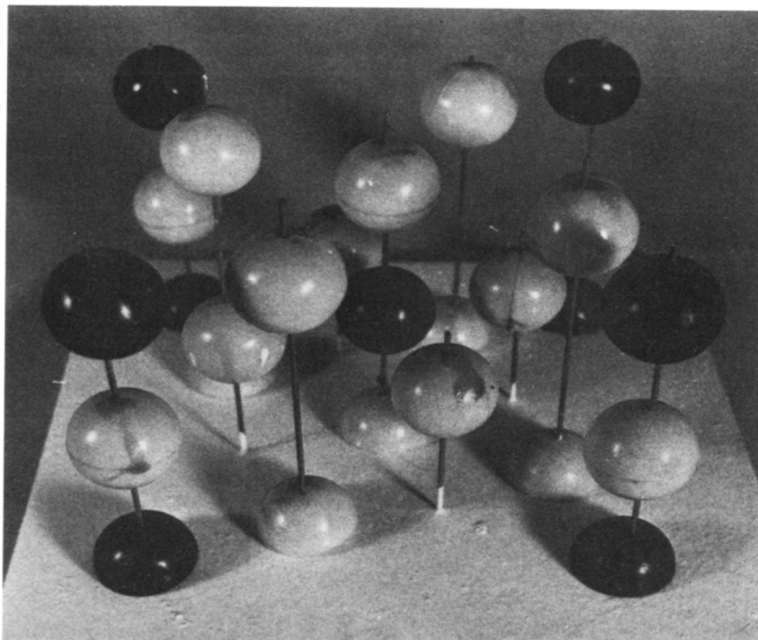
Fig. 12. A model of the α-UF₅ structure type.
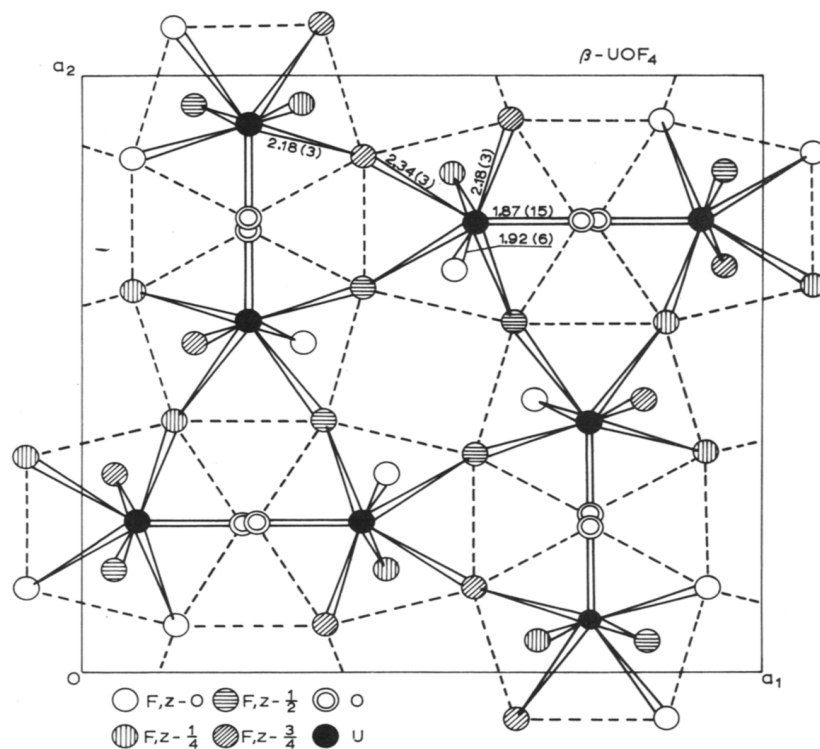
Fig. 13. The structure of β-UOF₄. The bridging scheme is the same as in the Zachariasen β-UF₅ structure [60].
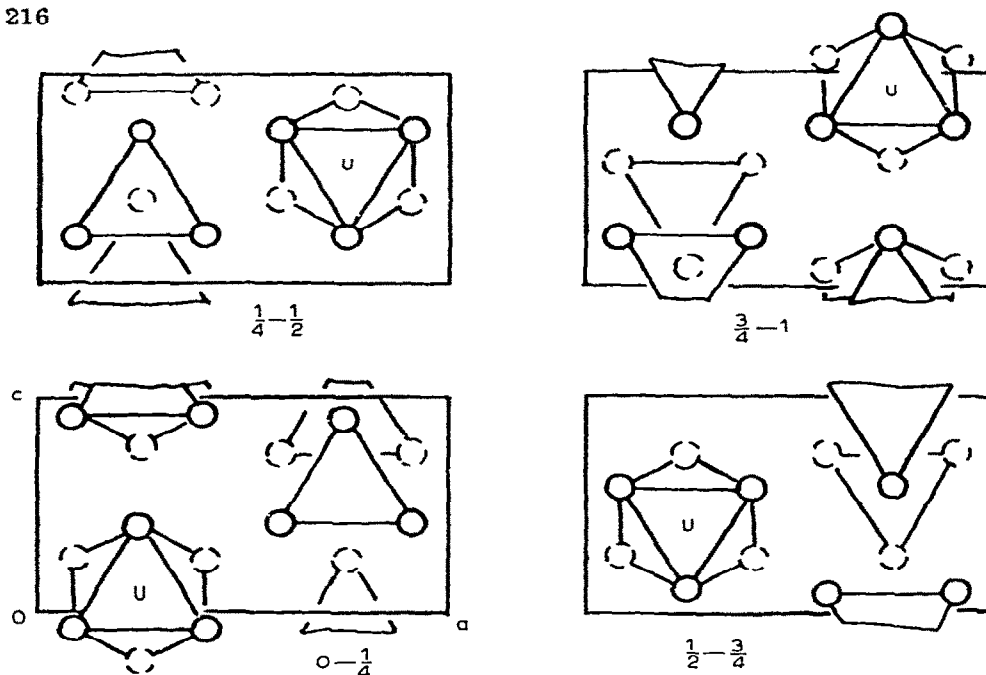
Fig. 14. The solid-state structure of UF_6, illustrating the hexagonal close packing of the fluorine atoms [18].
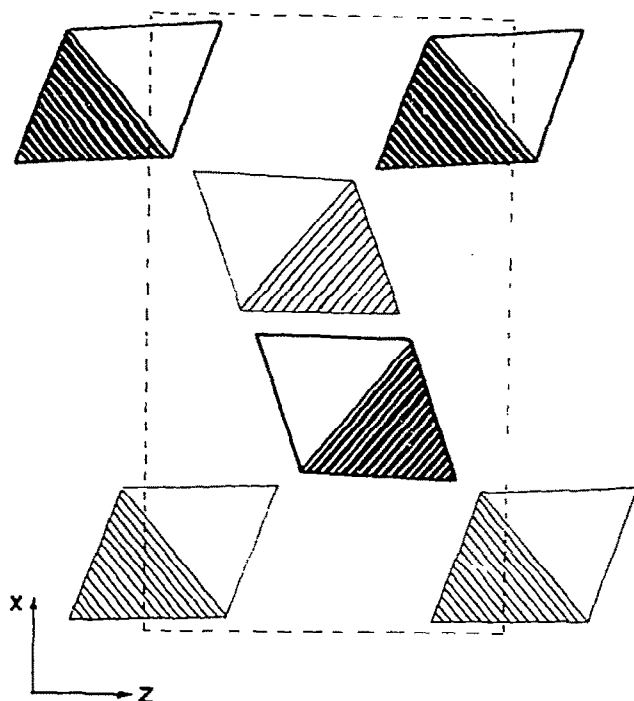
Fig. 15. The structure of UF_6 viewed as an assemblage of discrete octahedral UF_6 molecules. The octahedra on the mirror at $y = 1/4$ are lightly shaded, and on the mirror at $y = 3/4$ they are heavily shaded.
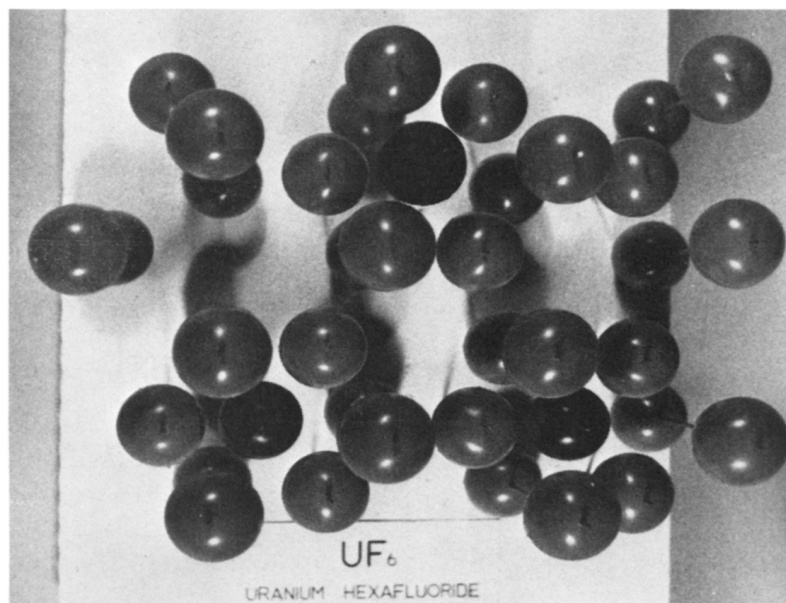
Fig. 16. A model of UF_6, seen down "a" (cf. Fig. 14).
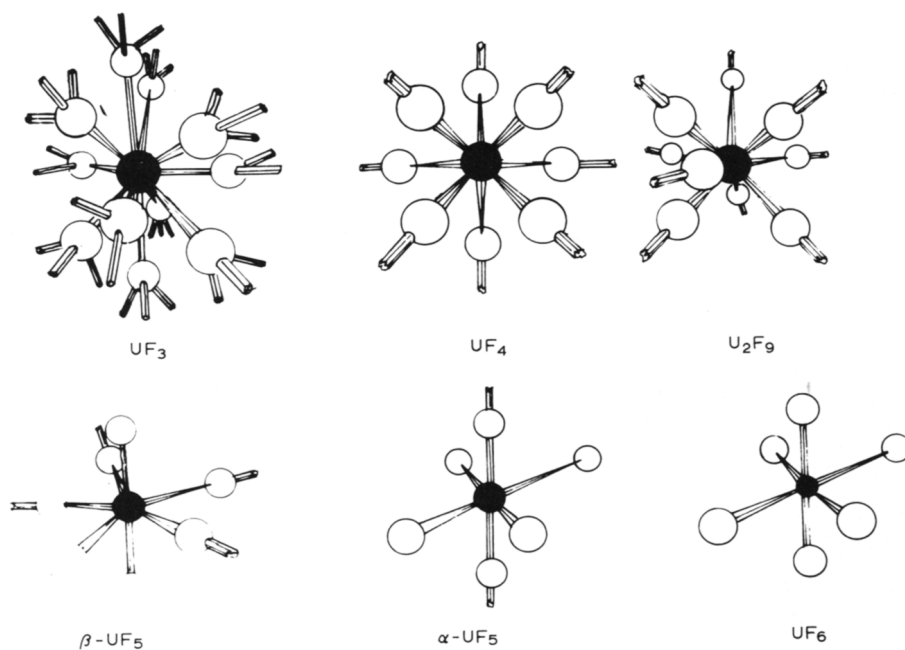
Fig. 17. Fluorine-bridging schemes in the solid-state structures of the series $UF_3 \rightarrow UF_6$.

TABLE 6

Correlation of amount of fluorine bridging in the structures of UF_3, UF_4, U_2F_9, UF_5 and UF_6 with some physical properties. Data taken from Brown [3]

	UF_3	UF_4	U_2F_9	β-UF_5	α-UF_5	UF_6
No. of U bound to a F atom	3,4	2	2	1,2	1,2	1
Vapour pressure at M.P. (kPa)	$\sim 10^{-4}$	0.6			1.7 [a]	152
Melting point (K)	$\sim 1700(d)$	1309			621	337
$-\Delta H_f$	351	450	473	491		523
Cp_{298}	~ 23	27.7			31.6	40.0
S_{298} (eu)	28	36	39		45	54

[a] Where it is uncertain whether the literature refers to α- or β-UF_5, the quantities are typed on the borderline.

(vii) Trends in the uranium binary halide structures and their correlation with some physical properties

The structures of UF_3, UF_4, U_2F_9, α-UF_5, β-UF_5 and UF_6 are shown in Fig. 17; the fluorine bridging schemes are depicted. Each broken bond from a bridging fluorine goes to a nearby uranium atom. The bridging schemes are quantitatively described in Table 5.

As the cation size decreases from UF_3 to UF_6, the polyhedral size and the amount of fluorine bridging also decrease. The covalent character of the bonds increases, until UF_6, a typical molecular crystal, is reached. In UF_3, the fluorine atoms are firmly trapped by uranium atoms, each being bonded to 3 or 4 uranium atoms. This would account for the high melting point. In UF_4 and the mixed-valence compound U_2F_9, each fluorine atom is bonded to 2 uranium atoms, whereas in α- and β-UF_5 terminal fluorine atoms appear. In UF_6, all fluorine atoms are terminal.

The fluorine bridging schemes (Fig. 16) explain trends in physical properties [3] such as melting point, volatility, heat capacity, etc., as listed in Table 6.

C. DIVALENT ACTINIDE HALIDE TYPES

Keller [6] lists the II oxidation state for uranium, and Ackermann and Rauh [65] report the metastable monoxides ThO and UO. However, in the absence of any knowledge of the electrical properties of UO, it may be preferable to specify the lower oxidation state of uranium as +3 or less (see also ref. 66). So far, no divalent halides have been reported for uranium but they have been reported for some higher actinides. $AmCl_2$, $AmBr_2$ and AmI_2 were

TABLE 7

Crystal data for $AmCl_2$, $AmBr_2$, AmI_2 and their isotypes

Compound	a (Å)	b (Å)	c (Å)	β (deg)	Space group	Structure type
$AmCl_2$	7.573	8.963	4.532		Pnma	$PbCl_2$, $EuCl_2$
$PbCl_2$	7.62	9.05	4.535		Pnma	
$AmBr_2$	11.592		7.121		Tetragonal	$SrBr_2$, $EuBr_2$
AmI_2	7.677	8.311	7.925	98.46	$P2_1/c$	EuI_2, m-ZrO_2
EuI_2	7.64	8.26	7.88	98	$P2_1/c$	
Monoclinic-ZrO_2	5.145	5.208	5.311	99.23	$P2_1/c$	

prepared [34,35] by reaction of the metal with the mercuric halide

$$M^0 + HgX_2 \xrightarrow[500°]{400°-} MX_2 + Hg^0$$
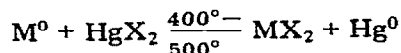
$AmCl_2$ is of the $PbCl_2$, $EuCl_2$ structure type [67], where the metal is 9-coordinate in a tricapped trigonal prism. $AmBr_2$ is said to be of the $SrBr_2$—$EuBr_2$ type [68,69], but the $SrBr_2$ analysis is an old one and should be repeated (it is not mentioned by Wyckoff [46]). AmI_2, however, is of the well characterised EuI_2 [70]—monoclinic ZrO_2 [71] type, where the C.N. is 7 and the polyhedron is square based and trigonal topped (Fig. 2). Crystal data for the actinide dihalides and their isotypes are summarised in Table 7. ThI_2, whose crystal structure has been reported [72], is formally divalent, but the bond lengths and other physical properties suggest that Th^{4+} ions are present in the lattice, the valency being satisfied by free electrons between the layers of the structure.

D. THE URANIUM TRIHALIDE STRUCTURE TYPES

The UF_3, UCl_3 and UI_3 structure types occur widely in the actinide and lanthanide trihalides, but not in the transition metal trihalides, the latter being too small to support the high C.N. values of 11, 9 and 8. Tables 2 and 3 show the distribution of these types over the actinide and lanthanide series. The 11-coordinate UF_3 type gives way to the 9-coordinate orthorhombic YF_3 type at BkF_3 in the actinide series [73,74] and between PmF_3 and SmF_3 in the lanthanide series [75]. Interestingly, the high-temperature form in the lanthanide and actinide trifluorides is the more dense UF_3 type, in contrast with the usual situation where the density decreases on transition to a high temperature form.

The actinide and lanthanide trichlorides, tribromides and triiodides undergo the following transitions in structure type as the trivalent cation size becomes smaller with the actinide or lanthanide contraction

Type $UCl_3 \rightarrow UI_3 \rightarrow AlCl_3 \rightarrow FeCl_3$

C.N. =   9   8   6   6

TABLE 8

Transition locations for the trihalide structure types

(a) Actinides-transition type [a]

	1 → 2	3 → 4	4 → 5	5 → 6	4 → 6
Trifluorides	BkF_3				
Trichlorides		$CfCl_3$ d			
Tribromides		$NpBr_3$ d	$BkBr_3$ t	$CfBr_3$ d	$BkBr_3$ t
Triiodides					AmI_3 d

(b) Lanthanides-transition type

	1 → 2	3 → 4	4 → 5	5 → 6	4 → 6
Trifluorides	Between PmF_3 and SmF_3				
Trichlorides		$GdCl_3$ d	$DyCl_3$ d		
Tribromides			$GdBr_3$ d		$GdBr_3$ d
Triiodides					SmI_3

[a] 1, UF_3-type; 2, YF_3-type; 3, UCl_3-type; 4, UI_3-type; 5, $AlCl_3$-type; 6, $FeCl_3$-type; d, dimorphic; t, trimorphic.

The AlCl$_3$ type has only recently been observed [76] for actinide trihalides, in BkBr$_3$ and CfBr$_3$, although it is well known in the lanthanide trichlorides. The structural transitions in the actinide and lanthanide trihalide series are summarised in Table 8.

(i) The UF$_3$ and YF$_3$ types

The present state of knowledge of the 11-coordinate UF$_3$ type has been fully discussed in Sect. B(i). In common with the LaF$_3$—UF$_3$ type, the YF$_3$ type also has a space-group ambiguity, the possible space groups being Pnma and Pn2$_1$a; however this is not troublesome, unlike the ambiguity in UF$_3$. Cheetham and Norman [77] refined the structure of YF$_3$ by neutron powder profile analysis and the YF$_3$ structure is shown in Fig. 18. The yttrium atom has been said to be 8-coordinate [78], but the neutron results clearly show that YF$_3$ is 9-coordinate. In the tricapped trigonal prism there are eight Y—F distances between 2.281(3) and 2.310(2) Å, while the ninth is only slightly withdrawn to 2.538 Å. The space-group ambiguity is unimportant here because a satisfactory structure is obtained in the higher symmetry space group Pnma, and there is no need to move the fluorine atoms off the mirror planes.
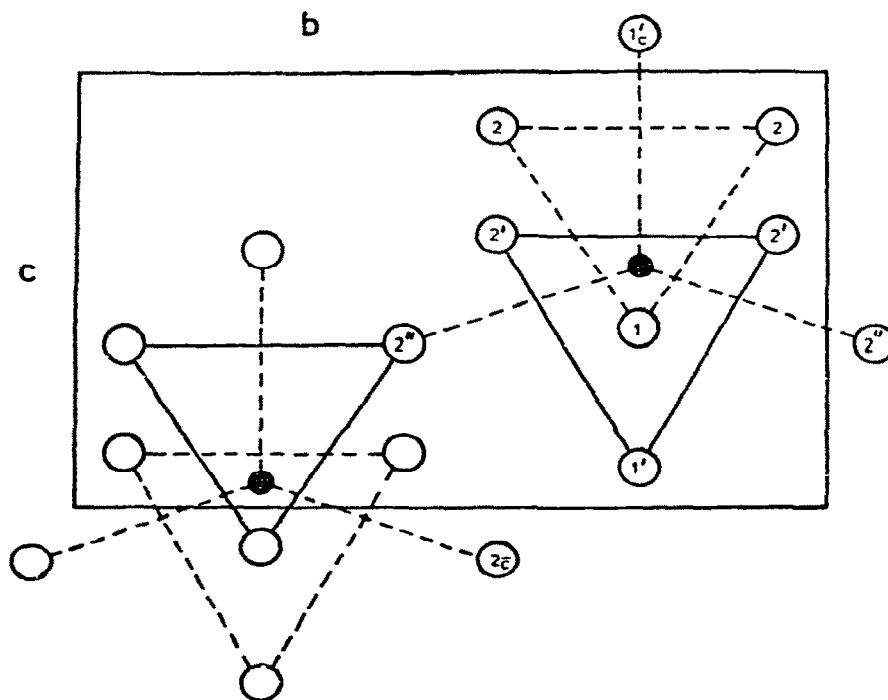
Fig. 18. Projection of the YF$_3$ structure down the *a*-axis. The Y atom is clearly surrounded by nine fluorine atoms in a tricapped trigonal prism arrangement (after Cheetham and Norman [77]).

TABLE 9

Unit cell data for LaF_3 and YF_3 types in the actinide series

Compound	a (Å)	b (Å)	c (Å)	Structure type
LaF_3	7.41		7.55	
UF_3	7.181		7.348	
NpF_3	7.129		7.288	
PuF_3	7.093		7.254	LaF_3-type-$P\bar{3}c1$ or $P6_3$ cm (trigonal
AmF_3	7.044		7.225	or hexagonal)
CmF_3	6.999		7.179	
BkF_3	6.97		7.140	
CfF_3	6.944		7.101	
BkF_3	6.70	7.09	4.410	
CfF_3	6.653	7.041	4.395	YF_3 type-$Pnma$ (orthorhombic)
YF_3	6.354	6.855	4.395	

BkF_3 and CfF_3 are dimorphic [73,74], showing the UF_3 and YF_3 structures, the YF_3 type being the low temperature form. Some unit cell data for the UF_3 and YF_3 type actinide trifluorides are given in Table 9.

(ii) The UCl_3 and UI_3 types

The UCl_3 structure was deduced from X-ray powder data by Zachariasen [79] in 1948. Recently, the structure was confirmed in a neutron diffraction study in this laboratory [9], and the halogen positions precisely determined. The structure of UCl_3 as viewed down the hexagonal c-axis, is shown in Fig. 19. The polyhedron is a symmetrically tricapped trigonal prism, whose C.N. is 9. Columns of trigonal prisms of chlorine atoms sharing end faces run in the c-direction, and each column is surrounded trigonally by three others, displaced by $c/2$. The chains are cross-linked; the prism atoms of one chain become the cap atoms of an adjacent chain. The UCl_3 coordination polyhedron is shown in Fig. 20, and the irregular environment of a chlorine atom in Fig. 21. The structure of UBr_3, isostructural [79,80] with UCl_3, was also refined in this laboratory by neutron profile analysis [10]. UBr_3 is adjacent to $NpBr_3$ which shows the UCl_3 and UI_3 types [80], however, UBr_3 does not transform to the UI_3 type on cooling to 77 K [81].

Levy et al. [11] studied the UI_3 structure by neutron diffraction profile analysis, and confirmed the $PuBr_3$ type first proposed for UI_3 by Zachariasen in 1948 [79]. The UI_3 structure is shown in Fig. 22. The coordination polyhedron is a bicapped trigonal prism, the third capping atom being withdrawn by bonding with a neighbouring uranium atom. The structure is layered in planes perpendicular to a. The U—I distances are 3.165(12) (2×), 3.244(8) (4×) and 3.456(11) (2×) Å, while the withdrawn iodine atom is 4.696(16) Å from the uranium atom, a distance too long for appreciable bonding. In UI_3, the prism base is an isosceles triangle rather than the equilateral triangle as in
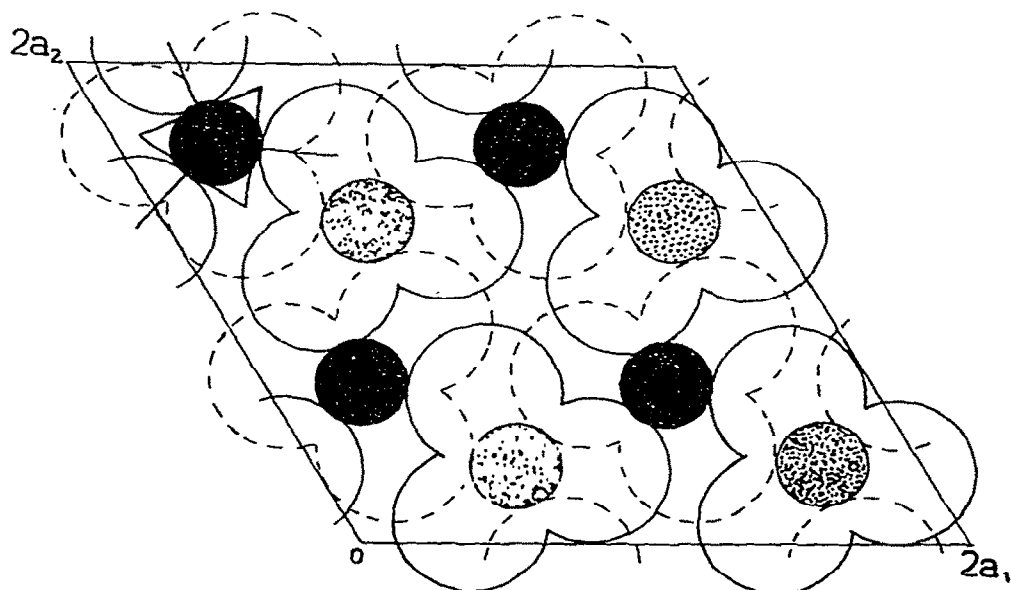
Fig. 19. The structure of UCl_3 seen down the hexagonal c-axis. The dark circles are U at $z = 0.75$ and the dotted circles U at $z = 0.25$. The full circles are Cl at $z = 0.75$ and dashed circles Cl at $z = 0.25$. The radii correspond to ionic radii. One tricapped trigonal prism is shown (from Taylor and Wilson [9]).
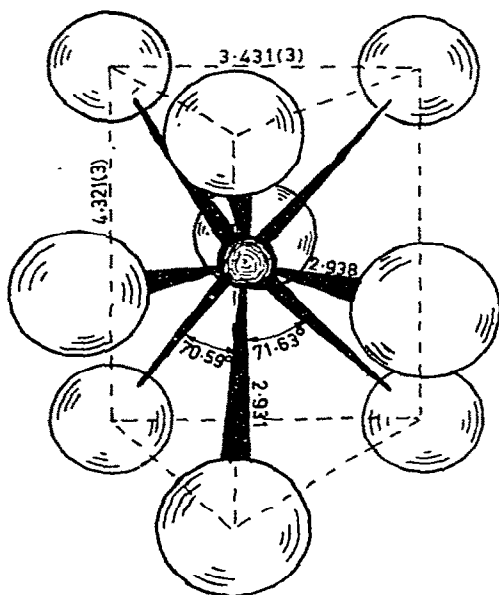
Fig. 20. The symmetrically tricapped trigonal prism configuration of chlorine atoms around the uranium atom in UCl_3 and UBr_3 (atom radii not to scale). Distances are for UCl_3 (after Taylor and Wilson [9,10]).
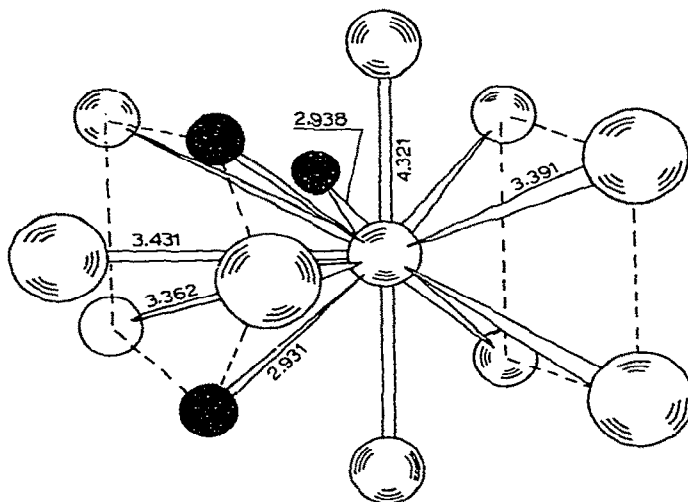
Fig. 21. The peculiar halogen atom environment in UCl_3 and UBr_3. Such irregular arrangements are common in the actinide halides. Distances as for UCl_3 (after Taylor and Wilson [9,10]).
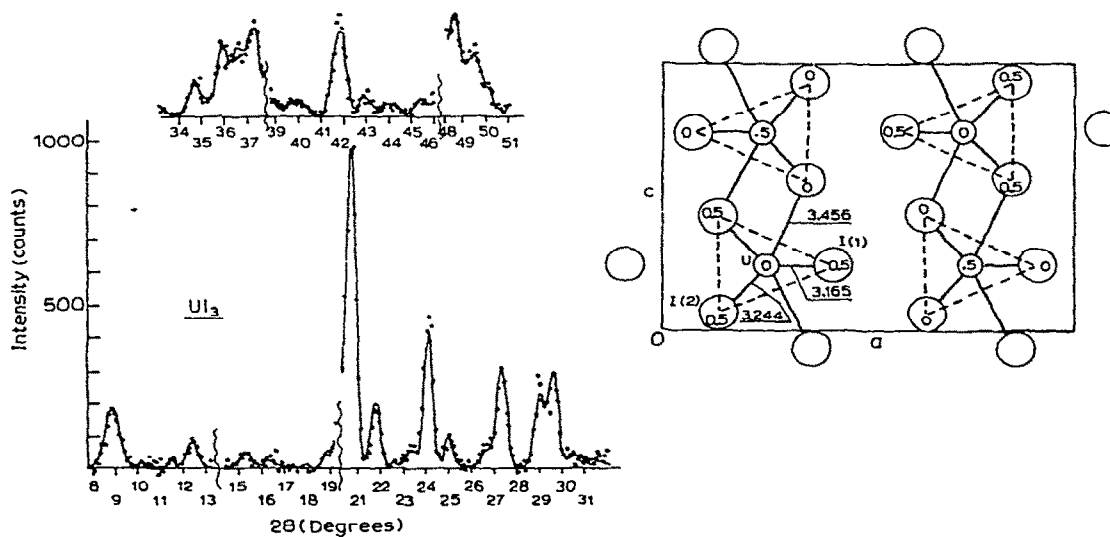
Fig. 22. The structure of UI_3. The y-coordinates of the atoms (0 or 0.5) are shown, and also the neutron powder pattern from which the coordinates were determined (after Levy et al. [11]).
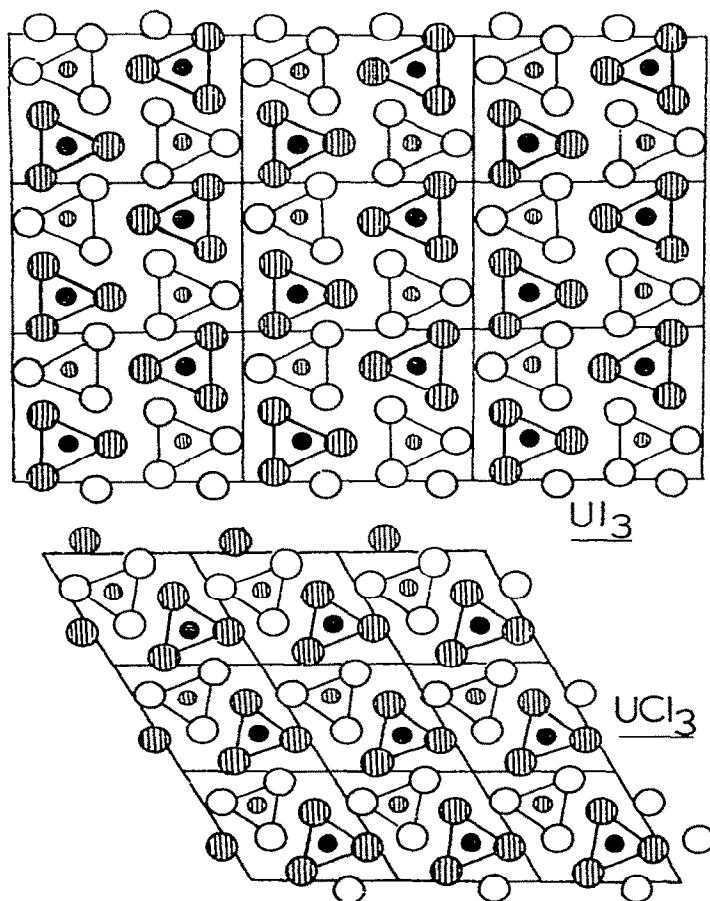
Fig. 23. Showing the close relationship between the UCl_3 and UI_3 types. The orientations of the prismatic columns differ slightly with the two types. It is seen that a transformation from one to the other could be effected by rotation of the prisms and rearrangement of the cap atoms.

UCl_3, and the U atom is 0.28 Å from the centroid of the prism.

The UI_3 type is compared with the UCl_3 type in Fig. 23. The two structures are closely related. The prismatic columns are lined up in orthogonal anti-parallel fashion in UI_3, but in UCl_3 the relative positions of the columns are somewhat different. A transformation from one type to the other could be effected by rearrangement of the capping bonds, e.g. in going from UCl_3 to UI_3, a third of the cap bonds would be broken and the remainder shifted. The anions are more efficiently packed in UI_3 than in UCl_3; the ratio of anionic volume ($\frac{4}{3}\pi r_x^3$) to volume per halogen atom in the unit cell is 0.72 for UCl_3 and 0.89 for UI_3.

The structural formulae are [$UCl_{6/3}$ (apical) $Cl_{3/3}$ (cap)] for UCl_3 and [$UI_{6/3}$ (apical) $Cl_{2/2}$ (cap)] for UI_3.

(iii) Structural transitions in the actinide and lanthanide trichlorides, tribromides and triiodides

Available structural data for the trihalides of the UCl_3 type are collected in Table 10. Careful single-crystal X-ray diffraction studies have been carried out on $PuCl_3$, $AmCl_3$, $CmCl_3$ and $CfCl_3$ by Burns and co-workers and others [76,82—85], and on the lanthanide compounds $LaCl_3$, $NdCl_3$, $EuCl_3$ and $GdCl_3$ by Morosin [86]. The unit cells show the actinide and lanthanide contractions, but the two variable positional parameters, x_{Cl} and y_{Cl} only change slightly. The apical and equatorial bonds are nearly equal for the trichlorides of the larger cations, but diverge as the cations get smaller. This is due to increasing instability in the equatorial cap bonds owing to the impending change to the UI_3 type, caused by withdrawal of one cap atom. In Fig. 24 the apical and equatorial bond lengths are plotted for the actinide and lanthanide trichlorides of the UCl_3 type as a function of metallic radius, the UCl_3 data being from Taylor and Wilson [9] and the remainder from Burns et al. [84]. The equatorial and apical bond lengths measured for UCl_3 in this laboratory by neutron diffraction [9] fall on the curve at a U^{3+} radius of 1.04 Å. The shorter apical bonds decrease monotonically with decreasing cation size, but the equatorial bonds go through a minimum and then rise slightly owing to the oncoming transition to the UI_3 type.

Burns et al. [84] found orthorhombic UI_3 type and hexagonal UCl_3 type
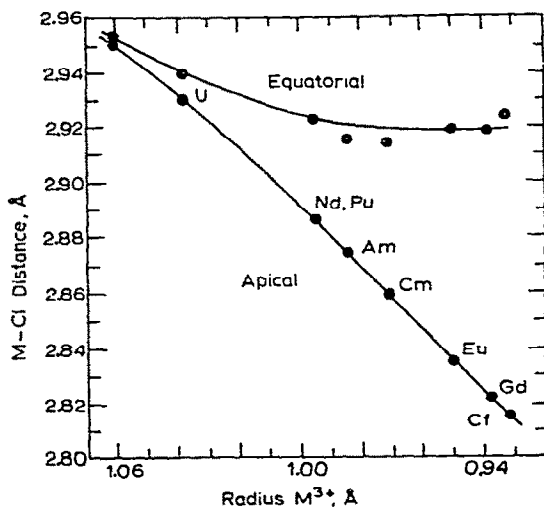
Fig. 24. Apical and equatorial M—Cl bond lengths in actinide and lanthanide trichlorides of the UCl_3 type [9,84].

TABLE 10

Presently known structural data for the UCl₃ structure types

Compound	a (Å)	c (Å)	$10^4\,x$	$10^4\,y$	M–X apical (Å)	M–X equatorial (Å)	r_{M^+} (Å)	MP (°C)
AcCl₃	7.62	4.55						
AcBr₃	8.076	4.689						
UCl₃	7.443	4.321	3858(4)	3009(4)	2.931(2)	2.938(3)	1.04	
UBr₃	7.942(2)	4.441(2)	3859(4)	2996(4)	3.062(2)	3.145(3)		
NpCl₃	7.413	4.282						
α-NpBr₃	7.916	4.390						
PuCl₃	7.394(1)	4.243(1)	3879(2)	3021(2)	2.886(1)	2.919(1)	0.995	
AmCl₃	7.382(1)	4.214(1)	3877(4)	3019(4)	2.874(2)	2.915(2)	0.984(3)	715
CmCl₃	7.3743(11)	4.1850(7)	3882(2)	3018(2)	2.9589(9)	2.9138(13)	0.971(3)	695(10)
BkCl₃	7.382	4.127						603
CfCl₃	7.379(1)	4.0900(5)	3902(6)	3019(6)	2.815(3)	2.924(4)	0.932(3)	545
EsCl₃	7.47 [a] (7.40)	4.10 [a] (4.07)						
LaCl₃	7.4779(5)	4.3745(5)	3874.1(21)	3015.5(21)	2.950(2)	2.953(2)	1.061	
NdCl₃	7.3988(9)	4.2423(6)	3877.7(24)	3016.7(24)	2.886(2)	2.923(2)	0.996	
EuCl₃	7.3746(12)	4.1323(5)	3891.1(23)	3017.4(23)	2.835(2)	2.919(2)	0.949	
GdCl₃	7.3663(9)	4.1059(4)	3892.9(25)	3015.3(25)	2.822(2)	2.918(2)	0.937	

[a] Parameters at 425°C. Room temperature parameters in parentheses.

TABLE 11

Presently known structural data for the UI$_3$ structure types

Compound	a (Å)	b (Å)	c (Å)	M–X prism (2X) (Å)	M–X prism (4X) (Å)	M–X Cap (2X) (Å)	M–X (withdrawn) (Å)
PaI$_3$	4.33	14.00	10.02				
UI$_3$	4.328(5)	14.011(16)	10.005(11)	3.165(12)	3.244(8)	3.456(11)	4.696(16)
β-NpBr$_3$	4.108	12.618	9.153				
NpI$_3$	4.326	13.980	9.982				
PuBr$_3$	4.097	12.617	9.147				
PuI$_3$	4.326	13.962	9.974				
AmBr$_3$	4.064	12.661	9.144				
α-AmI$_3$	4.31	14.03	9.92				
CmBr$_3$	4.041(2)	12.70(2)	9.135(3)	2.865(6)	2.983(4)	3.137(4)	4.318(9)
α-BkBr$_3$	4.03	12.71	9.12				
CfCl$_3$	3.869(2)	11.748(7)	8.561(4)	2.690(7)	2.806(4)	2.940(6)	4.005(9)
TbCl$_3$				2.70(2)	2.79(2)	2.95(2)	3.79(2)

TABLE 12

FeCl₃ structure types in the actinide trihalides

Compound	a (hex)^a Å	c (hex) Å	Space group	Rhombohedral cell	
				$a_{rh.}$ (Å)	α (deg)
FeCl₃	6.06	17.38	R$\bar{3}$	6.758	53.2
β-AmI₃	7.42	20.55	R$\bar{3}$	8.08	54.7
CmI₃	7.44	20.40	R$\bar{3}$	8.03	55.2
β-BkBr₃	7.26	19.23	R$\bar{3}$	7.66	56.6
BkI₃	7.50	20.40	R$\bar{3}$	8.06	55.4
α-CfBr₃	7.14	19.08	R$\bar{3}$	7.58	56.2
CfI₃	7.55	20.80	R$\bar{3}$	8.19	54.9

^{a} The triple hexagonal cell is given, as well as the true rhombohedral cell.

crystals of CfCl₃ growing in the same preparation under the same conditions. BkBr₃ was shown by Burns et al. [76] to be trimorphic, being found in the AlCl₃, UI₃ and FeCl₃ forms. CfBr₃ shows the AlCl₃ and FeCl₃ type structures [76].

In the AlCl₃ and FeCl₃ types, the cation is octahedrally coordinated, the anion packing being cubic close-packed in the former and hexagonal close-packed in the latter. The types interconvert readily by translational movements along one direction in a double layer containing the cations. CrCl₃ has the AlCl₃ structure at 298 K and the FeCl₃ structure at 225 K [87].

The crystal data for the UI₃ types are given in Table 11. Positional parameters for UI₃ were determined by neutron profile refinement [11], and for CmBr₃ [76] and CfCl₃ [84] by single-crystal X-ray diffraction. Some data for the AlCl₃ and FeCl₃ types are given in Tables 12 and 13.

E. THE URANIUM TETRAHALIDE STRUCTURE TYPES

Tables 2 and 3 show that the UF₄ structure type occurs widely in the actinide series and also for some transition metal and lanthanide fluorides. On

TABLE 13

AlCl₃ structure types in the actinide trihalides

Compound	a (Å)	b (Å)	c (Å)	β (deg)	Space group
AlCl₃	5.92	10.22	6.16	108	C2/m
β-CfBr₃	7.214	12.423	6.825	110.7	C2/m
γ-BkBr₃	7.23	12.53	6.83	110.6	C2/m

the other hand, the UCl_4 and UBr_4 structure types have only been observed for actinide compounds. The UI_4 type has not yet been characterised, but it is not isostructural with ThI_4, a unique structure described below.

(i) The UF_4 type

This structure type was first determined [55] for α-ZrF_4, and later the α-ZrF_4 type was found to occur with UF_4 [54]. The structure has been described in Sect. B(ii), the uranium atom being 8-coordinated in a distorted square antiprism (Fig. 8). A new cubic modification of UF_4 was prepared by Deribas et al. [56] by the action of compressive shock on UF_4 at 16—50 GPa and 400—1600°C, which could be converted to the usual monoclinic α-ZrF_4 form by reheating to 500°C. A second monoclinic form of ZrF_4 has been reported [88] but no corresponding polymorph of UF_4 has yet been found. The structure of UF_4 is complex and has a high lattice energy [89]. Unit cell data [3] for the tetrafluorides related to UF_4 are given in Table 14. Accurate lattice parameters for UF_4, BkF_4 and CfF_4 have been determined by Haug and Baybarz [205].

(ii) The UCl_4 type

In 1949, Mooney [90] proposed a structure for UCl_4 and the isostructural compound β-$ThCl_4$ from X-ray powder data. A neutron powder profile analysis by Taylor and Wilson [12] and a careful single-crystal X-ray study of isostructural β-$ThCl_4$ by Mucker et al. [91] showed that the chlorine positions

TABLE 14

Crystal data for tetrafluorides of the UF_4 type [1], [205]

Compound	a (Å)	b (Å)	c (Å)	β (deg)	Space group
α-ZrF_4 [a]	11.71	9.89	7.66	126.15	C2/c
HfF_4	11.68	9.84	7.62	126.1	C2/c
CeF_4	12.6	10.6	8.3	126	C2/c
ThF_4	12.90	10.93	8.58	126.4	C2/c
PaF_4	12.83	10.82	8.45	126.4	C2/c
UF_4	12.803	10.792	8.372	126.30	C2/c
NpF_4	12.64	10.70	8.36	126.4	C2/c
PuF_4	12.59	10.69	8.29	126.0	C2/c
AmF_4	12.56	10.58	8.25	125.9	C2/c
CmF_4	12.51	10.61	8.20	125.8	C2/c
BkF_4	12.396	10.466	8.118	126.33	C2/c
CfF_4	12.327	10.402	8.113	126.44	C2/c

[a] A second polymorph, β-ZrF_4, is monoclinic, with space group $P2_1$ or $P2_1/m$, with a = 15.82, b = 13.73, c = 15.11 Å and β = 106.25° [88].

determined by Mooney needed modification. The two later studies agreed
well and gave a more regular dodecahedral polyhedron than appeared from
the early work. The bond lengths and angles in UCl_4 and β-$ThCl_4$ found in
these determinations approached the dimensions of the "most favourable"
dodecahedron of Hoard and Silverton [92] calculated for a discrete dodeca-
hedron with minimum ligand repulsions. Brown et al. [93] refined atomic
coordinates in the isostructural Th, Pa, U and Np tetrachlorides and Th and
Pa tetrabromides, (UCl_4 type) using X-ray powder data. In their study it was
found that the chlorine and bromine positions could be refined in the pres-
ence of uranium with the X-ray integrated intensities but with a precision
about ten times less than the X-ray single-crystal [91] or neutron profile [12]
refinements.

The parameters from the various refinements of the UCl_4 type structures
are given in Table 15. Also given are the unit cell dimensions, the M—X dis-
tances d_A and d_B and the angles θ_A and θ_B these bonds make with the $\bar{4}$ axis,
for comparison with the predictions of the "hard sphere" and "most favour-
able" dodecahedron of Hoard and Silverton [92].

The UCl_4 structure is shown in Fig. 25(b). The dodecahedra have $\bar{4}2m$
symmetry and share edges to form a tetragonal three-dimensional framework.
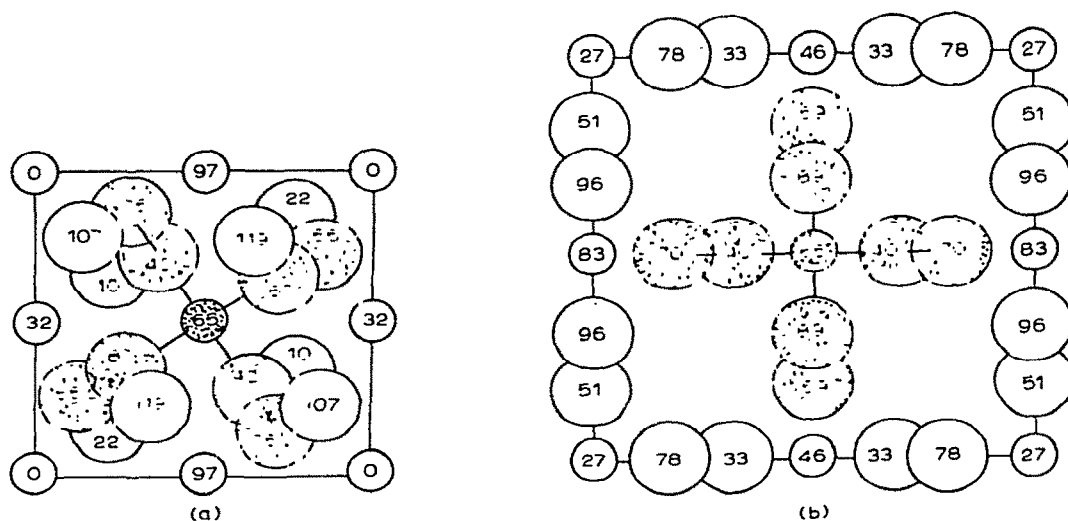
Fig. 25. (a) The α-$ThCl_4$, α-$ThBr_4$ structure type [32] (chlorine large circles, thorium
small circles). The heights above the cell base are shown in Å (origin of β-form raised 2.73
Å along c). The atoms in the central polyhedron are shaded. The two intersecting trapezoids
forming the dodecahedron are seen end-on. The view is down the tetragonal c-axis. (b) The
β-$ThCl_4$, UCl_4 structure type [32]. The dodecahedron is rotated 45° from the position in
the α-form. The view is again down the tetragonal c-axis. This high temperature form is
more open than the low temperature α form, having channels running along the lines (1/4,
1/4, z), etc. (after Mason et al. [32]).

TABLE 15

Structural data for UCl$_4$ and its isotypes β-ThCl$_4$ and β-ThBr$_4$, compared with data for the polymorphic modifications, α-ThCl$_4$ and α-ThBr$_4$

Compound	a (Å)	c (Å)	Space group	d_A (Å)	d_B (Å)	d_A/d_B	θ_A (deg)	θ_B (deg)
UCl$_4$ [12]	8.296	7.487	I4$_1$/amd	2.869	2.638	1.088	32.66(9)	77.94(7)
β-ThCl$_4$ [91]	8.473	7.468	I4$_1$/amd	2.90	2.72	1.07	33.1	78.0
β-ThBr$_4$ [33]	8.934	7.964	I4$_1$/amd	3.12	2.85	1.10	32.8	77.3
PaCl$_4$ [93]	8.377	7.482	I4$_1$/amd	2.95	2.64	1.12	33.3	76.9
NpCl$_4$ [93]	8.250	7.460	I4$_1$/amd	2.93	2.60	1.12	32.9	76.8
PaBr$_4$ [93]	8.824	7.957	I4$_1$/amd	3.07	2.77	1.11	33.7	78.2
α-ThCl$_4$ [32]	6.408	12.924	I4$_1$/a	2.89	2.85	1.01	38.3	69.8
α-ThBr$_4$ [33]	6.737	13.601	I4$_1$/a	3.02	2.91	1.04	37.9	69.5
Hard sphere model						1.00	36.9	69.5
Most favourable dodeca- hedron model						1.05	35.2	73.5

TABLE 16

Crystal data for the UBr₄ types UBr₄ and NpBr₄

Compound	a (Å)	b (Å)	c (Å)	β (deg)	Space group
UBr₄ [96], [26]	10.92	8.69	7.05	93.15	C2/m
NpBr₄ [1]	10.89	8.74	7.05	94.19	C2/m

(iii) Polymorphism in ThCl₄ and ThBr₄

Chiotti et al. [94] found polymorphism in ThCl₄ in calorimetric studies. Scaife [95] reported two forms of ThBr₄, but Brown et al. [93] obtained only the usual UCl₄ type for ThBr₄. Mason et al. [33] confirmed the dimorphism in ThBr₄. ThCl₄ and ThBr₄ show dimorphism between similar α(low) and β(high) temperature forms, the transformation temperature being 405°C for ThCl₄ and 426°C for ThBr₄. The high temperature β-forms are isostructural with UCl₄ and tetragonal, with space group I4₁/amd, and the cell dimensions given in Table 15. The low temperature α-forms are also tetragonal, but with space group I4₁/a and different cell dimensions, as shown in Table 15. Both α- and β-forms have four formula units per cell. The crystal structures of the α-forms were solved by Mason et al. from X-ray powder and single-crystal data [32,33]. The α- and β-forms are compared in Figs. 25(a) and (b). The ThX₈ dodecahedra in both forms are similar but pack differently, the packing being more efficient in the low temperature α-form. Large channels run parallel to c in the β-form, but these collapse in the formation of the α-form. The polyhedra change shape slightly in going from β to α. In the higher symmetry β-form, the dodecahedra have $\bar{4}$2m symmetry, and in the α-form $\bar{4}$ symmetry. Table 15 shows that the dodecahedra in the low temperature α-form conform with the "hard sphere" model, whereas in the β-form the dodecahedra conform more with the "most favourable" dodecahedron of Hoard and Silverton [92].

(iv) The UBr₄ type

Table 2 shows that UBr₄ and NpBr₄ represent yet another actinide tetrahalide structure type. The monoclinic cell dimensions for UBr₄ have been known [96] since 1957 (see Table 16), but the structure defied solution until recently because UBr₄ does not grow to a crystal size suitable for single-crystal structure analysis. UBr₄ is monoclinic, with space group C2/m. Taylor and Wilson [25,26] recently solved this structure from the X-ray and neutron powder data. The uranium atoms were located relative to the two-fold axes by inspection of the X-ray intensities, and a structure model, deduced by trial-and-error methods, refined with the neutron powder profile technique. This
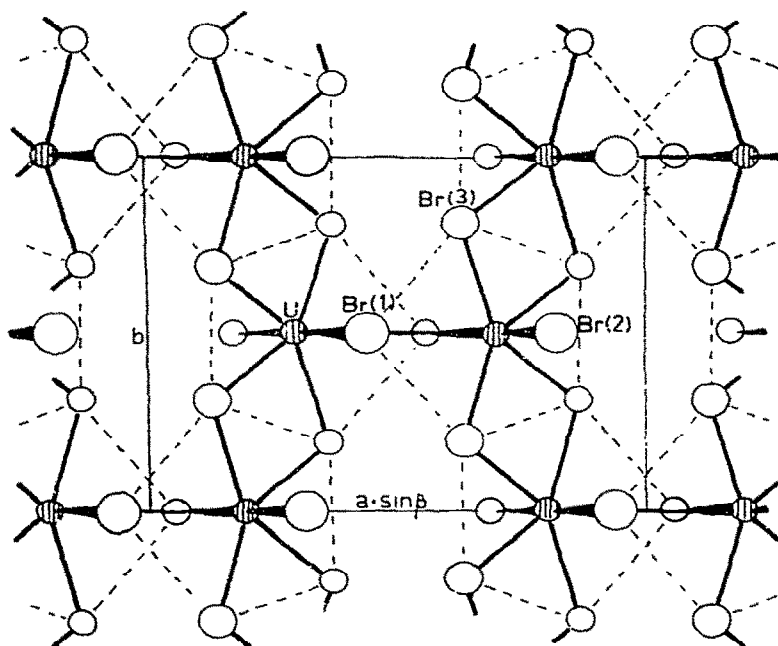
Fig. 26. The crystal structure of UBr$_4$ in the (ab) projection, showing the bonding of the pentagonal bipyramid chains into infinite sheets through the dual-purpose Br(1) atoms.
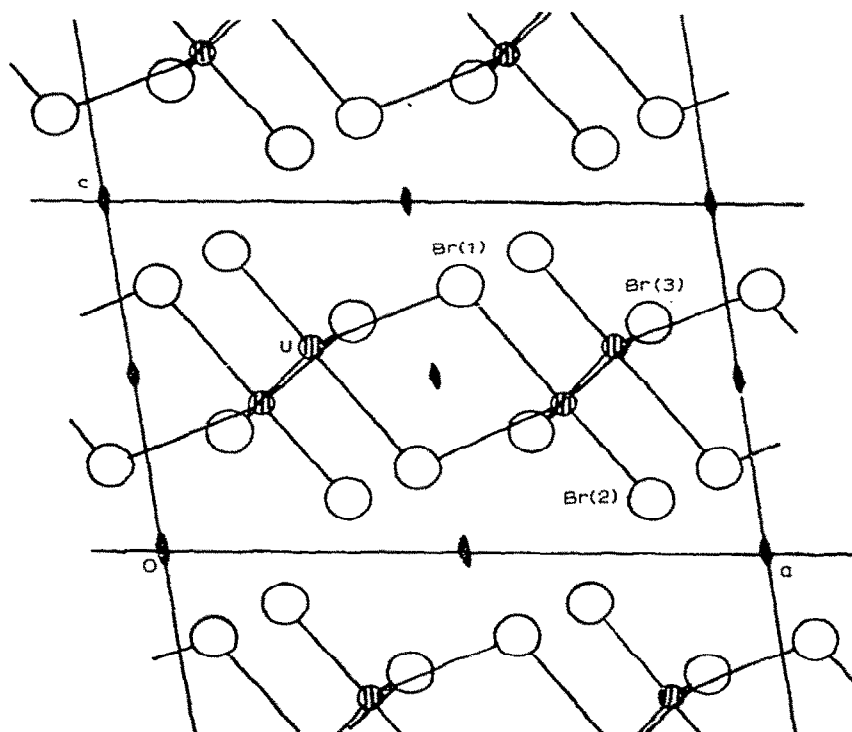
Fig. 27. The structure of UBr$_4$ viewed along b, illustrating the packing of the UBr$_4$ sheets, the intersheet bonding being of the van der Waals' type only.
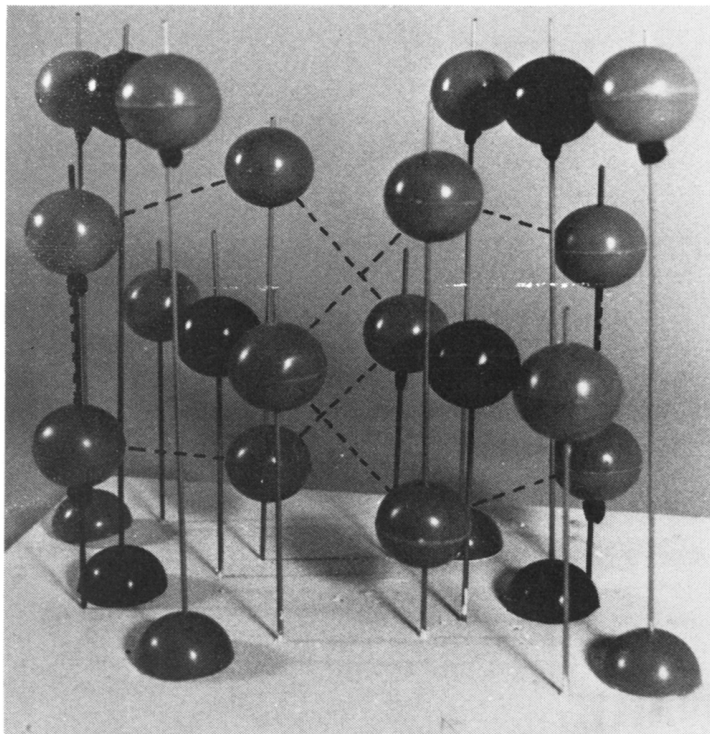
Fig. 28. A model of the UBr$_4$ structure, viewed along c. The equatorial pentagons are outlined.

new MX$_4$ structure type is illustrated in Figs. 26—28.

The UBr$_4$ structure is based on strings of edge-fused pentagonal bipyramids running parallel to b, the chains being cross-linked into sheets parallel to the (001) plane by means of the dual function bromine atom Br(1), which acts as an apical bromine atom in one sheet and a pentagonal ring bromine atom in the other sheet. The other apical atom, Br(2), is terminal. The short U—U vectors of ~ 4.5 Å are all double bromine-bridged. The structure is reminiscent of the anhydrous UO$_2$Cl$_2$ structure (see Sect. H(v)), where dual-role oxygen atoms are apical in one bipyramid and equatorial in the other. However, the bridging scheme is different in UO$_2$Cl$_2$, with single oxygen bridges, resulting in a quite different three-dimensional network of bonds in UO$_2$Cl$_2$. The UBr$_4$ sheets are only bonded together in the crystal by van der Waals' forces, and the structure is not based on close packing of anions. The structural formula is [UBrBr$_{6/2}$].

(v) The ThI$_4$ type

It is convenient here to discuss briefly the interesting and unique structure [97] shown by ThI$_4$. ThI$_4$ is monoclinic, space group P2$_1$/n, with 4 molecules
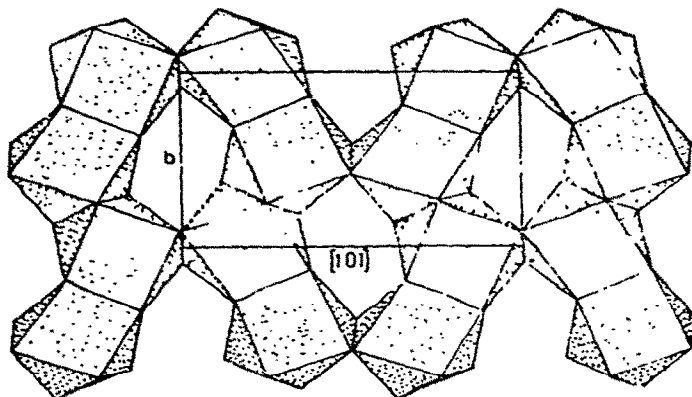
Fig. 29. One layer of the ThI_4 structure [97] showing edge and triangular-face-linked polyhedra. The polyhedra have variously been described as distorted square antiprisms or dodecahedra [43].

per unit cell of dimensions $a = 13.216(7)$, $b = 8.068(6)$ and $c = 7.766(6)$ Å and $\beta = 98.68(5)°$. Like UBr_4, ThI_4 forms a layered structure with only weak intralayer forces, but there are eight iodine atoms around the thorium atom. The polyhedron is intermediate, having been described both as distorted square antiprismatic and dodecahedral [43]. The identical polyhedra share edges and triangular faces to form the layers shown in Fig. 29. The ThI_4 structure is $[ThI_{8/2}]$. As in UBr_4, the anion packing in the layers is not simple. UI_4 is not
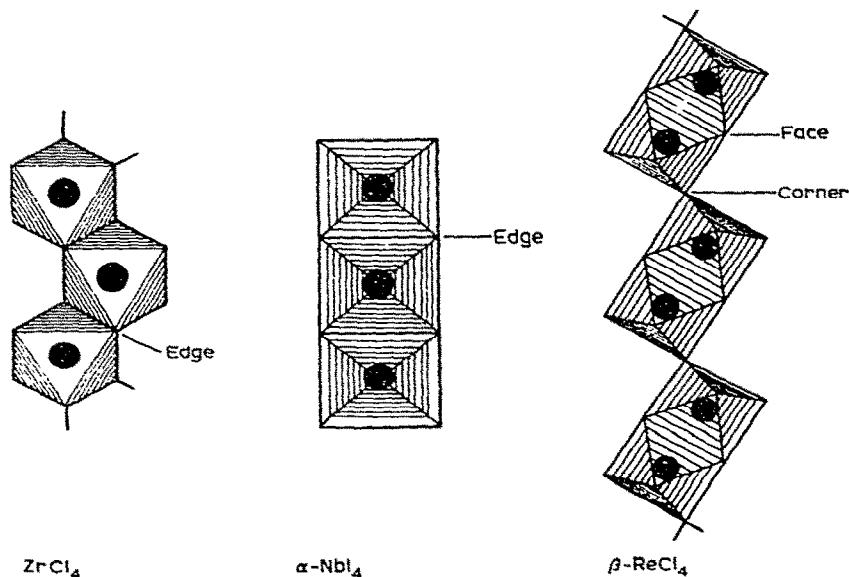
Fig. 30. Known transition metal tetrahalide structure types.

TABLE 17

Summary of coordination polyhedra found around U^{4+} in some UF_4—alkali fluoride complexes

U^{4+} compound	Crystal system	Space group	C.N.	Polyhedron type
LiUF$_5$ [98]	Tetragonal	I4$_1$/a	9	Tricapped trigonal prism. Adjacent prisms share edges and corners
β_1-K$_2$UF$_6$ [99,7] β_1-K$_2$ThF$_6$ [99,7] β_1-K$_2$NpF$_6$ [7,100] Rb$_2$ThF$_6$ [7,101]	Hexagonal	P$\bar{6}$2m	9	Tricapped trigonal prism. Basal face-sharing.
KU$_2$F$_9$ [58]	Orthorhombic	Pnma	9	Tricapped trigonal prism, with edge sharing.
CsU$_2$F$_9$ [59]	Monoclinic	C2/c	8½	Tricapped trigonal prism, one prism corner statistically only half-occupied. Corner sharing.
NaTh$_2$F$_9$ [42]	Cubic	I$\bar{4}$3m	9	U$_2$F$_9$ type structure with Na atom in octahedral hole. Tricapped trigonal prism with all corners shared.
(NH$_4$)$_4$UF$_8$ [102]	Monoclinic	C2/c	8	Isolated dodecahedra.
Rb$_2$UF$_6$ [103]	Orthorhombic	Cmcm	8	Edge-sharing dodecahedra.
Li$_4$UF$_8$ [104]	Orthorhombic	Pnma	8	Isolated polyhedra. Tricapped trigonal prism —1.
K$_7$Th$_6$F$_{31}$ [105] Na$_7$Zr$_6$F$_{31}$ [106] (isomorphous with Na$_7$U$_6$F$_{31}$ [7] K$_7$U$_6$F$_{31}$ [7] Rb$_7$U$_6$F$_{31}$ [7] (NH$_4$)$_7$U$_6$F$_{31}$ [7])	Rhombohedral	R$\bar{3}$	8	Square antiprisms sharing corners, with one fluorine atom in a cavity.

isostructural [3] with ThI$_4$. The Th—I distances are quite regular, lying in the range 3.13—3.29 Å.

(vi) Coordination polyhedra in some alkali fluoride complexes of tetravalent uranium

Some of the coordination polyhedra found in these compounds are shown in Table 17. The same typical polyhedra, e.g. tricapped trigonal prisms, dodecahedra and square antiprisms, are found as in the binary halide series. However, the addition of the alkali halide tends to depolymerise the parent binary actinide halide [7].

(vii) Comparison of actinide and transition metal tetrahalide structure types

Because the transition metal +4 ions are smaller than the actinide +4 ions (Fig. 1), ZrF$_4$ and HfF$_4$ are the only transition metal tetrahalides showing isomorphism with actinide tetrahalides. The transition metal halides were reviewed recently by Walton [107]. The ZrF$_4$ type structures have already been described (Sect. B(ii)). The remaining transition metal tetrahalide structure types consist of infinite chains of octahedra, linked by edges, corners and faces. In ZrCl$_4$ [108], ZrBr$_4$ [108], HfCl$_4$ [108], HfBr$_4$ [108], and TcCl$_4$ [109], the octahedra are edge-shared (Fig. 30), the unshared anions being *cis*-related. In a second type, typified by α-NbI$_4$ [110], opposite edges are shared (Fig. 30). There is a short Nb—Nb distance (3.31 Å) in α-NbI$_4$. NbCl$_4$, NbBr$_4$, TaCl$_4$, TaBr$_4$, TaI$_4$, WCl$_4$ and WBr$_4$ are probably of this type [107]. MoCl$_4$ is dimorphic, probably showing the ZrCl$_4$ and α-NbI$_4$ types [107]. A third type [111] is shown by β-ReCl$_4$ (Fig. 30) where bi-octahedra Re$_2$Cl$_9$ share faces, the bi-octahedra being linked at corners into infinite chains.

F. THE URANIUM PENTAHALIDE STRUCTURE TYPES

(i) The α-UF$_5$ and β-UF$_5$ types

These have been described in the uranium binary fluoride series (Sect. B(iv), (v)).

(ii) The α-UCl$_5$ and β-UCl$_5$ types

The pentahalides of uranium, most of the other actinides and the transition metals, except the fluorides, are generally built up from M$_2$X$_{10}$ molecular dimers. They are all based on the close packing of halogens (h.c.p. or c.c.p.) and there is a wide variety in the number of arrangements formed by the dimers. Some of the pentahalides, including UCl$_5$, are dimorphic.

α-UCl$_5$ was prepared by Smith et al. [112] by reacting U$_3$O$_8$ with CCl$_4$ at 400°C and cooling the saturated solution of UCl$_5$ in CCl$_4$ from 100°C to room

temperature over 2 h. Smith et al. [112] showed that this form was based on cubic close-packed anions with uranium in one fifth of the octahedral holes, in such a way as to give U_2Cl_{10} dimers. The α-UCl_5 structure is illustrated in Fig. 31(a) and (b). Figure 31(a) shows the view down the crystal a-axis, which is nearly coincident with the pseudo cubic (a') axis, the Cl atoms being seen in a f.c.c. arrangement. Figure 31(b) shows the view down a pseudo hexagonal (c') axis, normal to the hexagonal chlorine layers. In this view, the dimers are
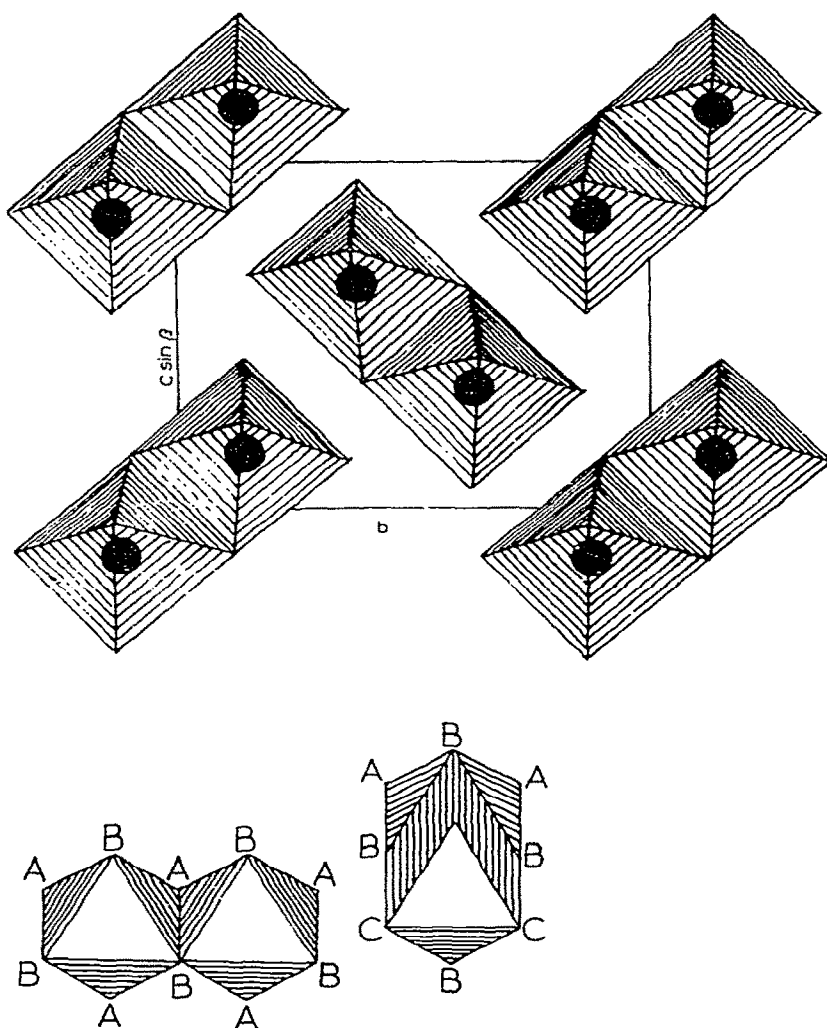
Fig. 31. (a) The structure of the monoclinic form α-UCl_5 in the a-axis projection, showing the U_2Cl_{10} dimers. (b) Two adjacent and identical dimers seen when the α-UCl_5 structure is viewed normal to the h.c.p. anion layers. The different orientations arise as the dimers are seen down different molecular three-fold axes.
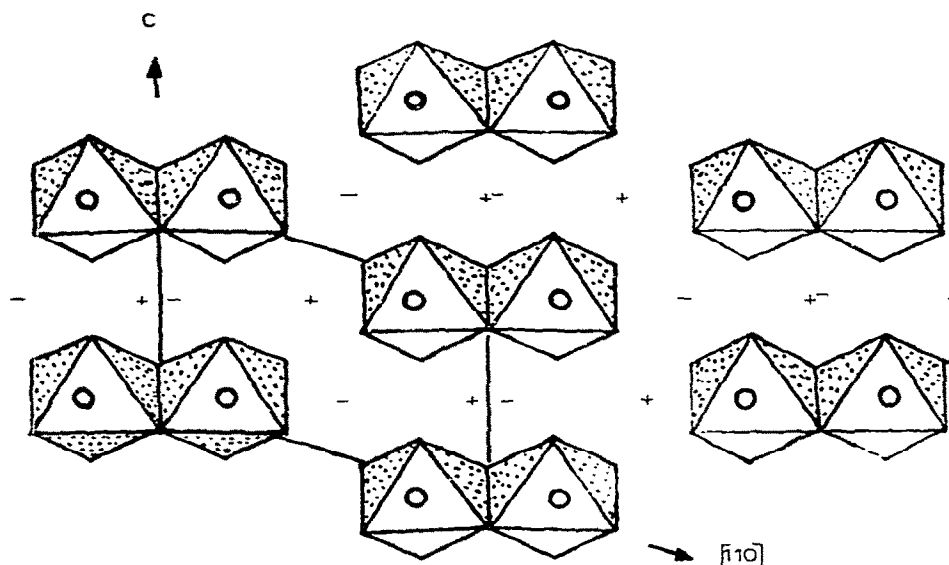
Fig. 32. The crystal structure of the triclinic form β-UCl$_5$, showing two of the close packed layers and the dimeric molecules U$_2$Cl$_{10}$. The + and − signs indicate which octahedral holes are filled between adjoining layers above and below the layers shown to give the adjacent dimers [31].

seen in two orientations; in some dimers the two uranium atoms are between the same sheets and in others they are between different sheets.

The β-form of UCl$_5$, which is triclinic, was prepared by Müller and Kolitsch [31], by slow reduction of UCl$_6$ with CH$_2$Cl$_2$ at room temperature, and also by long standing of UCl$_6$ solutions at room temperature. This form is based on simple h.c. packing of the anions and the β-UCl$_5$ structure is illustrated in Fig. 32. Although the volume per molecule in the two modifications is about the same (362 × 10^{-30} m^3 for α, 360 × 10^{-30} m^3 for β), probably β-UCl$_5$ is the low and α-UCl$_5$ the high temperature form. By comparing Figs. 31 and 32, it can be seen that the dimers in a cell are parallel to each other and to the h.c.p. layers in the β-form and are perpendicular to each other and the pseudo cubic a-axis in the α-form.

(iii) The UBr$_5$ type

UBr$_5$ is isostructural [113] with α-PaBr$_5$ (see Sect. F(iv) below), but the structure is unknown.

(iv) The protoactinium pentahalide types

PaCl$_5$ seems unique in the actinide and transition metal pentahalides (except fluorides) in that it is not based on dimers. The structure [114] consists
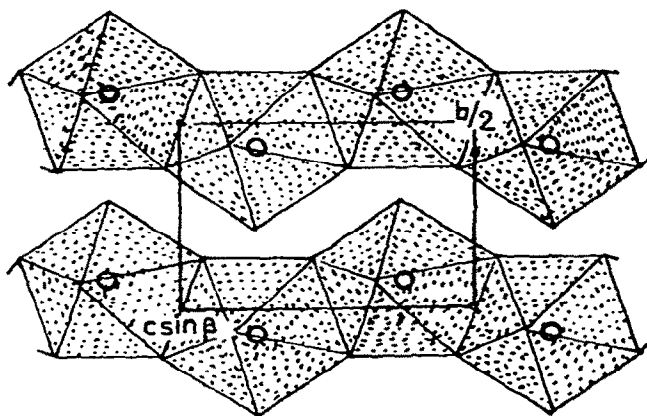
Fig. 33. The structure of PaCl$_5$, showing the infinite chains, made up of edge-fused pentagonal bipyramids [114].

of infinite chains of edge-fused pentagonal bipyramids, as shown in Fig. 33. The chains are only bonded by van der Waals' forces, and packed side by side in a hexagonal arrangement when viewed along the chains. The PaCl$_5$ structure is thus fibrous.

PaBr$_5$ has two modifications [115]. Sublimation at 400—410°C gives β-PaBr$_5$ and at 390—400°C gives α-PaBr$_5$, the capillaries always containing one modification only [115]. The low α-form, which is isostructural with UBr$_5$, can be transformed to β-PaBr$_5$ [115]. The structure of the β-form was found [115] to be of the α-UCl$_5$ type (see Sect. F(ii)).
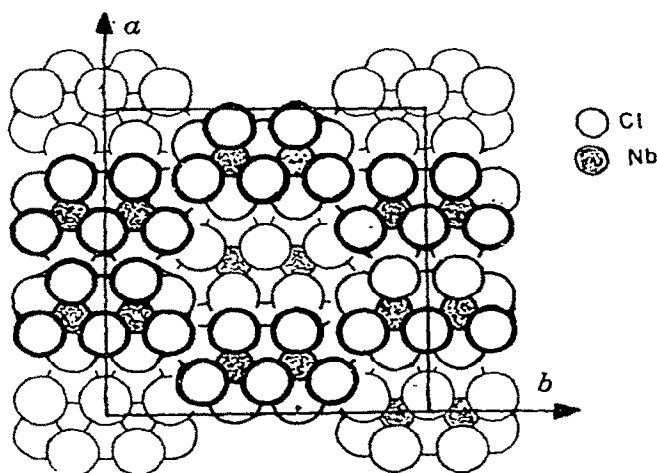
Fig. 34. The packing of the Nb$_2$Cl$_{10}$ groups in the niobium pentachloride structure [116].

(v) Comparison of actinide and transition metal pentahalide types, except fluorides

NbCl₅ [116], TaCl₅ [116], NbBr₅ [117,107], TaBr₅ [107], MoCl₅ [117], WCl₅ [107], ReCl₅ [118], NbI₅ [107], TaI₅ [107], WBr₅ [107] and ReBr₅ [107] all have structures based on M_2Cl_{10} dimers. Surprisingly, none reproduce the UCl₅ and PaBr₅ types described above. The dimers appear to exist in solution, but in the vapour phases, MoCl₅, NbCl₅ and NbBr₅ are trigonal bipyramids [116,117]. SbCl₅ in the solid is trigonal bipyramidal [119].

NbCl₅, TaCl₅ and MoCl₅ are isostructural [116]. They have monoclinic cells (Table 21) and M_2Cl_{10} dimers with a h.c.p. anion array. The NbCl₅ structure type is shown in Fig. 34, which shows the packing of the dimers.

ReCl₅ shows yet another structure type [118] with M_2X_{10} dimers. It is monoclinic, space group P2₁/c, with double h.c.p. anion packing ABAC ⋯ The ReCl₅ structure is shown in Fig. 35. The dimers pack in a parallel array. Table 18 compares the efficiency of the dimer packing in the pentahalide structure types TaCl₅, ReCl₅, β-UCl₅ and α-UCl₅. The β-UCl₅ type is the more
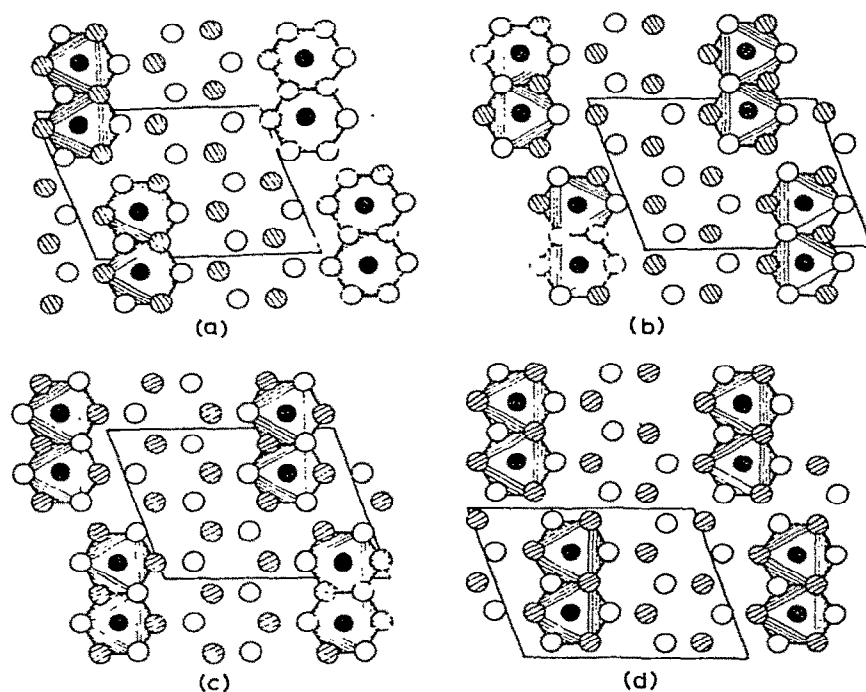
Fig. 35. The ReCl₅ structure, showing the packing of the Re atoms into the double h.c.p. chlorine layers, forming parallel Re_2Cl_{10} molecular dimers [118]. (a), (b), (c) and (d) show the 0—1/4, 1/4—1/2, 1/2—3/4 and 3/4—1 layers, respectively. The unit cell is outlined and with the origin at the lower left, c is to the right and a upwards.

TABLE 18

Molecular packing in the structure types TaCl$_5$, ReCl$_5$, α- and β-UCl$_5$

Type	ReCl$_5$	TaCl$_5$	α-UCl$_5$	β-UCl$_5$
Volume per Cl atom (Å^3)	30.3	32.3	36.0	36.3
M—Cl bridge (Å)	2.47	2.56	2.70	2.68
M—Cl terminal (Å)	2.24	2.28	2.43	2.44
M···M in dimer (Å)	3.74	3.95	4.16	4.17
Chlorine packing	d.h.c.p.	h.c.p.	h.c.p.	c.c.p.

open type, with a greater volume per chlorine atom in the crystal, but not much greater than in α-UCl$_5$. As the volumes per chlorine atom in ReCl$_5$ and TaCl$_5$ are lower than in UCl$_5$, high temperature forms for these compounds may be possible. The crystal data for these actinide and transition metal pentahalides are given in Table 19.

(vi) The transition metal pentafluoride types and isostructural oxy-tetra-fluorides

So far, no pentafluorides of the 1st, 2nd and 3rd row transition metals have been found to be isostructural with the known actinide pentafluoride types
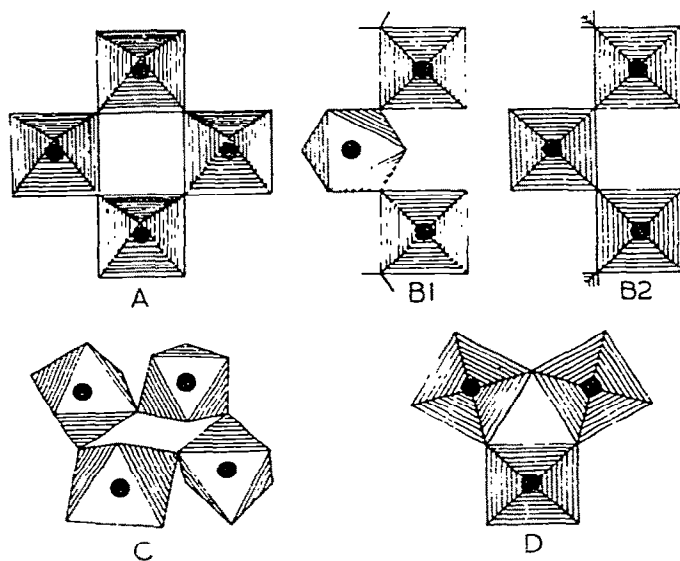
Fig. 36. The three structural types in the transition metal pentafluorides: (A) tetramers with linear fluorine bridges, (B1 and B2) MF$_5$ chains with *cis*-bridging and (C) tetramers with nonlinear fluorine bridging. The trimeric type (D) oxy-tetrafluoride type is also shown. See Table 20 for examples of the various types.

TABLE 19

Summary of actinide and transition metal pentahalide structure types

Compound	Cell				Space group	Anion packing	Structure type[a]
	a	b	c	β			
NbF$_5$, MoF$_5$, TaF$_5$, WF$_5$ }						Distorted c.c.p.	A
VF$_5$, CrF$_5$, TcF$_5$, ReF$_5$ }		See Table 21			See Table 21	Intermediate	B2
RuF$_5$, RhF$_5$, OsF$_5$, IrF$_5$, PtF$_5$ }						Distorted h.c.p.	C
α-UF$_5$ [60]	6.512		4.463		I4/m	c.c.p.	E
BiF$_5$ [61]					I4/m	c.c.p.	E
WOCl$_4$ [62]	8.48		3.99		I4	c.c.p.	E
WOBr$_4$ [62]	8.96		3.93		I4	c.c.p.	E
β-UF$_5$ [60]	11.450		5.198		I$\bar{4}$2d		F
PaF$_5$ [63]	11.53		5.19		I$\bar{4}$2d		F
β-UOF$_4$ [30]	11.4743		5.2043		I$\bar{4}$2d		F
α-UCl$_5$ [112]	7.99	10.69	8.48	91.5	P2$_1$/n	c.c.p.	G
β-PaBr$_5$ [115]	8.385	11.205	8.950	91.1	P2$_1$/n	c.c.p.	G
β-UCl$_5$ [31]	Triclinic					h.c.p.	
α-PaBr$_5$ [115]	12.69	12.82	9.92	108	P2$_1$/c	Unknown	I
UBr$_5$ [113]						Unknown	I
PaCl$_5$ [114]	7.97	11.35	8.36	106.4	C2/c	Irregular	K
NbCl$_5$ [116]	18.30	17.96	5.888	90.6	C2/m	h.c.p.	L
TaCl$_5$ [116]	18.30	17.96	5.888	90.6	C2/m	h.c.p.	L
MoCl$_5$ [117]	17.31	17.81	6.079	95.7	C2/m	h.c.p.	L
WCl$_5$ [107]							L
ReCl$_5$ [118]	9.24	11.54	12.03	109.1	P2$_1$/c	d.h.c.p.	M

[a] A, NbF$_5$; B2, VF$_5$; C, RuF$_5$; E, α-UF$_5$; F, β-UF$_5$; G, α-UCl$_5$; H, β-UCl$_5$; I, α-PaBr$_5$; J, β-PaBr$_5$; K, PaCl$_5$; L, NbCl$_5$; M, ReCl$_5$.

α- and β-UF$_5$, although BiF$_5$ is isostructural with α-UF$_5$ (Table 3). In all the transition metal pentahalides, the metal is octahedrally surrounded by fluorine atoms, and three main structural types have been found:

(A) M$_4$X$_{20}$ tetramers with linear fluorine bridging and c.c.p. anions.

(B) Endless MF$_5$ chains with cis-bridging in an approximate h.c.p. array of anions. We have subdivided (B) into (B1) and (B2) types, because there are different relative orientations of the cis-bridging octahedra, the extreme cases B1 and B2 being shown in Fig. 36. This would explain why all the cis-bridged pentafluorides and oxy-tetrafluorides are not rigorously isostructural.

(C) M$_4$X$_{20}$ tetramers with non-linear fluorine bridging and h.c.p. anions.

The three structural types A—C are shown in Fig. 36. There is a correlation between structure type and position in the Periodic Table (Table 20). The crystallographic data for the pentafluorides and isomorphous oxy-tetrafluorides are shown in Table 21. A fourth type, D, which is shown by β-MoOF$_4$ and β-TcOF$_4$, is trimeric; so far, trimeric forms of the pentafluorides have not been observed. Type D is also shown in Fig. 36. It would appear that the last word has not yet been said on the pentahalide and oxy-tetrahalide structure types as Paine and Asprey [134] found that their ReF$_5$ and OsF$_5$ X-ray patterns could not be indexed from the literature data.

The M—F—M angles at the bridging fluorine atoms are shown in Table 22. Morrell et al. [135] consider the bonding changes from largely ionic to covalent through A → B → C, since the fluorine atom in type C is tending towards tetrahedral with two lone pairs, and the changes in structure type across a row (Table 20), are attributed to the effect of increasing nuclear charge.

(vii) Summary of the actinide and transition metal pentahalide structure types

Table 19 summarises the structure types of the actinide and transition metal pentahalides.

TABLE 20

Correlation of transition metal pentahalide structure types with metal position in the periodic table

VF$_5$	CrF$_5$				
B	B				
NbF$_5$	MoF$_5$	TcF$_5$	RuF$_5$	RhF$_5$	
A	A	B	C	C	
TaF$_5$	WF$_5$	ReF$_5$	OsF$_5$	IrF$_5$	PtF$_5$
A	A	B	C	C	C

TABLE 21

Crystallographic data for transition metal pentafluorides and isostructural oxy-tetrafluorides

Compound	Ref.	a	b	c	β	Space group	Structure type
NbF$_5$	120	9.62	14.43	5.12	96.1	C2/m	A
MoF$_5$	121	9.61	14.22	5.16	94.3	C2/m	A
TaF$_5$	120	9.64	14.45	5.12	96.3	C2/m	A
WF$_5$	122	9.61	14.26	5.23	94.6	C2/m	A
WOF$_4$	123	9.65	14.42	5.15	95.4	C2/m	A (disordered oxygens?)
VF$_5$	124	5.40	16.72	7.53		Pmcn	B2
CrF$_5$	125	5.5	16.3	7.4		Pmcn	B2
TcF$_5$	126	5.76	17.01	7.75		Pmcn	B2
ReF$_5$	127	5.70	17.23	7.67		Pmcn	B2
MoOF$_4$	128	5.50	16.98	7.84	91.7	P2$_1$/c	B2
α-TcOF$_4$	129	18.83	5.49	14.43	114.0	C2/c	B1
ReOF$_4$	130	19.01	5.57	14.72	114.0	C2/c	B1
α-CrOF$_4$	125	12.3	5.4	7.3	104		B
RuF$_5$	127	12.47	10.01	5.42	99.8	P2$_1$/a	C
RhF$_5$	135	12.34	9.92	5.52	100.4	P2$_1$/a	C
OsF$_5$	126, 131	12.59	9.91	5.53	99.5	P2$_1$/a	C
IrF$_5$	126	12.5	10.0	5.4	99.8	P2$_1$/a	C
PtF$_5$	126						?
β-TcOF$_4$	132	9.00		7.92		P6$_3$/m	D
β-MoOF$_4$	132	8.95		7.91		P6$_3$/m	D
β-CrOF$_4$	133						Unknown

TABLE 22

Bond angles at the bridging fluorine atoms in transition metal pentafluoride structure types A, B, C

Compound	Type	M—F—M (deg)	Fluorine packing
NbF$_5$	A	172(2)	~c.c.p.
VF$_5$	B	150	Intermediate, closer to h.c.p.
RhF$_5$	C	135(2)	h.c.p.

G. THE URANIUM HEXAHALIDE STRUCTURE TYPES

(i) The UF$_6$ type

In the actinides, UF$_6$, NpF$_6$ and PuF$_6$ form an isostructural series [18—20, 136,137] and the structure of UF$_6$ was solved by single-crystal X-ray analysis by Hoard and Stroupe [64] in 1958. Formally, the UF$_6$ type is based on h.c.p. anion layers with metal atoms in octahedral holes, the octahedra being discrete. The UF$_6$ structure, illustrated from the point of view of this packing scheme, is shown in Fig. 14. The unit cells [3] of UF$_6$, NpF$_6$ and PuF$_6$ are given in Table 23 and, strangely, do not follow the actinide contraction.

The fluorine atoms were more precisely located in neutron powder profile studies by Taylor et al. [18,19]. Finally, when a large single crystal of UF$_6$ became available, Levy et al. [20] carried out a high-precision single-crystal neutron diffraction study of UF$_6$ with 475 independent reflexions, which

TABLE 23

Crystallographic data for the orthorhombic UF$_6$ type hexafluorides (space group Pnma)

Compound	a	b	c	Temp. (K)	Ref.
MoF$_6$	9.559	8.668	5.015	193	21
TcF$_6$	9.55	8.74	5.02	254	140
RuF$_6$	9.44	8.59	4.98	243	140
RhF$_6$	9.40	8.54	4.96	250	140
WF$_6$	9.603	8.713	5.044	193	23
ReF$_6$	9.61	8.76	5.06	251	140
OsF$_6$	9.59	8.75	5.04	252	140
IrF$_6$	9.58	8.73	5.04	262	140
PtF$_6$	9.55	8.71	5.03	262	140
UF$_6$	9.843	8.920	5.173	193	19
UF$_6$	9.900	8.962	5.207	293	64
NpF$_6$	9.910	8.97	5.21	293	136
PuF$_6$	9.95	9.02	5.26	293	137

gave U—F distances precise to ±0.004 Å and anisotropic β_{ij} thermal parameters precise to ±5%. The last study shows a UF_6 molecule marginally distorted from regularity, with U—F distances of 1.996(4) and 2.004(4) Å in the mirror planes and 1.993(3) (2X) and 1.992(3) (2X) Å about the mirror planes. The slight distortions can be explained on the basis of the asymmetry of the U—U interactions. This agrees with an NMR study which gave one long and two short axes in solid UF_6 [138]. The F—F distances in the octahedra, 2.784(6)—2.806(3) Å are slightly longer than the fluorine ionic sum, so the fluorine atom arrangement around uranium is not strained. The F—U—F angles in the molecule, 89.42(17)—90.20(11)°, are nearly 90°. The U—F bonding has covalent character, as the U—F distances are less than the sum of the U^{6+} and F^- ionic radii, 2.08 Å.

In Table 24, the U—F distances obtained by the neutron powder, neutron single-crystal and X-ray methods are compared. The neutron single-crystal and powder studies agree to within a few e.s.d., but the single-crystal errors are several times less. The fluorine positions from the X-ray method were imprecise because of the large X-ray scattering power of uranium.

Analysis of the β_{ij} parameters from the neutron study gave some interesting results. The uranium atom vibration is nearly isotropic, but all the fluorines show the same type of anisotropic vibration. The shortest axes, $R1$, of the fluorine vibration ellipsoids are all precisely aligned along the U—F bonds, and r.m.s. displacements of 0.18—0.19 Å in this direction are the same as the uranium displacement. Normal to the bonds, the r.m.s. displacements along $R2$ and $R3$ are larger and nearly isotropic perpendicular to the bond with displacements of 0.239—0.264 Å. Analysis of the β_{ij} with the Cruickshank procedure [139] gave nearly perfect rigid body motion for the octahedra, the least-squares fit between observed and calculated β_{ij} giving an R-factor of 0.04 for rigid body motion. The r.m.s. amplitude of the rigid-body motion was 4.5°, showing that the UF_6 molecular librations were hindered.

The neutron studies show that the UF_6 structure is molecular, rather than

TABLE 24

Observed U—F distances in the various diffraction studies of crystalline UF_6

Bond	Study		
	Neutron single [a] crystal, 293 K	Neutron powder [b] profile, 193 K	The Hoard and Stroupe X-ray study, 1958
U—F(1)	1.996(4)	1.95(1)	2.13
U—F(2)	2.004(4)	2.03(2)	2.12
U—F(3) (2X)	1.993(3)	1.97(1)	2.02(5)
U—F(4) (2X)	1.992(3)	1.98(2)	2.02(5)

[a] Ref. 20; [b] Ref. 19.

ionic. The octahedra are discrete, with no corner, face or edge sharing (Fig. 15), which accounts for the high volatility of UF_6, a physical property which makes it important in the nuclear power industry.

(ii) UF_6 types in the transition metal hexahalides

As the uranium atom is much smaller in the hexavalent state, it is not surprising to find that the UF_6 type is widespread in the transition metal hexahalides. Siegel and Northrop deduced from X-ray powder photographs that MoF_6, TcF_6, RuF_6, RhF_6, WF_6, ReF_6, OsF_6, IrF_6 and PtF_6 were isostructural with UF_6, but their patterns were not suitable for structural analysis [140]. The compounds being moisture-sensitive and volatile, it was necessary to take the photographs of samples in capillary tubes at low temperatures. The unit cell data for the hexafluorides and experimental temperatures are given in Table 23. Low temperature neutron powder profile studies by Levy et al. [141,142] confirmed the UF_6 type for MoF_6 and WF_6 and provided the first measured positional parameters in the transition metal hexafluorides. The Mo—F and W—F bonds in the orthorhombic UF_6 type phases are both 1.81 Å, so the molecules in the transition metal hexafluorides are more compact and the fluorine atoms more compressed than in UF_6. The distances between the molecules however, are about the same in MoF_6, WF_6 and UF_6 (Table 25).

TABLE 25

Some comparisons arising from the neutron profile studies of the orthorhombic phases of MoF_6, WF_6 and UF_6 at 193 K

Quantity	o—MoF_6	o—WF_6	o—UF_6
(rM$^+$ + rF$^-$) (ionic radii sum) (Å)	1.93	1.91	2.08
M—F (average of observed) (Å)	1.81	1.81	1.98
Ionic sum (Å) — (M—F) (Å)	0.12	0.10	0.10
Ionic radius ratio	0.451	0.436	0.564
Mean (F—F) distance in octahedron (Å)	2.56	2.56	2.80
Mean F—F distance between molecules (Å)	3.10	3.12	3.11
Molecular volume $4/3\ \pi r^3$ (Å^3)	130	130	152
Ratio (unit cell volume/ 4 X molecular volume)	0.80	0.81	0.76
Molecular Debye—Waller factor (Å^2)	2.5(1)	3.14(8)	1.9(1)
R.m.s. amplitude of vibration, $(B/8\pi^2)^{1/2}$ (Å)	0.179(3)	0.200(3)	0.155(3)

TABLE 26

Crystallographic data and critical temperatures for the hexafluoride body-centred cubic plastic-crystal phases

Compound	Ref.	Cubic cell edge, a (Å)	Cell measurement temperature (K)	Orthorhombic-cubic transition temperature (K)	M.p. (K)
MoF$_6$	22	6.221	266	263.6	290.6
TcF$_6$	140	6.16	283	267.9	310.2
RuF$_6$	140	6.11	298	275.7	327.2
RhF$_6$	140	6.13	298	a	a
WF$_6$	24	6.30	268	264.7	275.1
ReF$_6$	140	6.26	283	269.7	291.7
OsF$_6$	140	6.25	298	274.6	306.4
IrF$_6$	140	6.23	298	272.0	317.2
PtF$_6$	140	6.21	298	276.2	334.5
SF$_6$	147	5.915	193	93	222.4

a Not given, Ref. 140.

The transition metal hexafluorides and SF$_6$, SeF$_6$ and TeF$_6$ have a plastic body-centred cubic phase between the melting point and the onset of the UF$_6$ type phase [138,140,143,144—146]. Unit cell data and transition temperatures are listed in Table 26. Neutron powder profile studies have been carried out at Lucas Heights on cubic MoF$_6$, WF$_6$ and SF$_6$ [22,24,147]. The cubic cells are bimolecular with molecules centred at (000) and ($\frac{1}{2}\frac{1}{2}\frac{1}{2}$). The fluorine distributions are disordered and curved owing to large librations of the molecules. The observed neutron powder data could not be fitted by conventional molecular models. The disordered fluorine distributions were described by Kubic Harmonic functions [148], K_m, on the surface of a sphere of radius the M—F distance, the expression for the fluorine density being of the form $\Sigma\, a_m K_m \delta\ (r—c)$, the delta function constraining the fluorine centre to lie on the spherical surface. The amplitude coefficients a_m were determined by least-squares fit. Only terms up to $m = 2$ were needed, as the smeared-out fluorine density had maxima along the unit cell edges. The refined values of the M—F distances in these plastic-crystal phases agreed well with the M—F distances in the low UF$_6$ type phases and with electron diffraction measurements in the vapour phase [149—151].

The results did not correspond to free rotation of the molecules which would require $a_2 = 0$. The Kubic Harmonic results, summarised in Table 27, show non-zero values for a_2, and insignificant higher order terms. The cell sizes are also incompatible with free rotation. For perfect b.c.c. packing, the spheres would be in contact along [111] and slightly apart along [100]. In WF$_6$, the distance from (000) to ($\frac{1}{2}\frac{1}{2}\frac{1}{2}$) would be 2 (W—F) + 2$r$(F$^-$) = 6.32 Å for sphere packing, whereas a smaller distance, $\sqrt{3}$ a/2 = 5.46 Å, is observed.

TABLE 27

Kubic harmonic profile refinements of neutron powder data for the cubic plastic phases of MoF_6, WF_6 and SF_6

Compound	Ref.	Coefficient a_2 [a]	M—F (Å)	B (Å^2)	M—F by electron diffraction [b]
MoF_6	22	4.65(16)	1.802(14)	9.1(5)	1.830
WF_6	24	4.83(24)	1.83(2)	10(1)	1.826
SF_6	147	5.93(11)	1.537(4)	5.5(2)	1.564(10)

[a] From the fluorine distribution function which is $1 + a_2 \{(x^4 + y^4 + z^4)/(M—F)^4 - 3/5\}$.
[b] See Refs. 149—151.

The a-axis length for sphere packing is 7.30 Å, implying a volume expansion of 80% at the orthorhombic—cubic transition, but only a 15% expansion occurs.

The abnormally high thermal B-factors measured in cubic MoF_6, WF_6 and SF_6 also suggest molecular disordering, and are in agreement with NMR results [138,144—146] which indicate fast reorientation and slow diffusion of the molecules. Less frequent reorientations occur in the orthorhombic phases of MoF_6 and WF_6 and in UF_6, which does not give the plastic phase.

From the above series of neutron diffraction studies, some interesting comparisons emerge (Table 25). The M—F bonds show covalent character, all being about 0.1 Å less than the ionic radii sums. The F—F distance in UF_6 is 0.1 Å longer than the ionic F—F contact distance, but 0.1 Å less in MoF_6 and WF_6, so the transition metal molecules are more strained than the UF_6 molecule. The SF_6 molecule is particularly strained. The librations of the UF_6 molecules were found to be hindered in the single-crystal neutron study. This would explain why UF_6 does not have a plastic phase below its triple point of 337.2; the U—F bonds are too long for large librations to occur. However, with the more compact MoF_6 and WF_6 molecules, the potential barrier for a molecular reorientation is more readily overcome.

All the neutron studies of the hexafluorides are compatible with a molecular lattice having weak attractions between molecules with molecular librations and reorientations, and high volatility in the solid state. O'Donnell et al. [152] found the chemical reactivity to be in the order $UF_6 > MoF_6 > WF_6$ and pointed out the differences in bonding in the two series (d^2sp^3 in MoF_6 and WF_6 and d^2sf^3 (?) in UF_6).

(iii) The UCl₆ type

The only actinide hexahalide known other than UF_6 is UCl_6, whose structure was determined [153] by Zachariasen in 1948 from X-ray powder data,

TABLE 28

Crystallographic data for the metal hexachlorides

Compound	a (Å)	c (Å)	α (deg)	Space group	M—Cl (Å)	Ref.
UCl_6	10.95	6.016		$P\bar{3}m1$	2.41—2.51	14
β-WCl_6	10.493	5.725		$P\bar{3}m1$	2.23—2.34	15
α-WCl_6	6.58		55.0	$R\bar{3}$	2.24	154

and refined by Taylor and Wilson [14] with the neutron powder profile technique. β-WCl_6 is isostructural with UCl_6 and the β-WCl_6 structure was also refined by Taylor and Wilson [15] by the neutron profile method. The crystal data for UCl_6 and α- and β-WCl_6 are summarised in Table 28.

The UCl_6 and α-WCl_6 [154] types are both based on h.c.p. chlorine layers with the metal atoms in one-sixth of the octahedral holes. The two structures are illustrated in Figs. 37—39. Taylor and Wilson pointed out that the chlorine layers are oriented in the same way relative to the three-fold axes and mirror planes in both types [15]; the only difference is due to the metal arrangement. In α-WCl_6, the W—W distances are all 6.58 Å, but in β-WCl_6, they are 6.07, 6.61 and 6.80 Å. The high β-WCl_6 form is retained at room temperature by rapid quenching, but it reverts to the blue α-WCl_6 on gentle heating.

The Cl—Cl contacts in UCl_6 and β-WCl_6 are compared in Table 29. The chlorine atoms contract about occupied octahedral holes and expand about those which are vacant. The disparity of the M—Cl bonds in these high forms parallels the Th—X bond disparities in high β-$ThCl_4$ and β-$ThBr_4$ (Sect. E(iii)). UCl_6 and WCl_6 are moderately volatile (7.7 kPa for UCl_6 and 5.7 kPa for WCl_6 at 215°C); UCl_6 sublimes at 100°C and 0.015 Pa.

Canterford and Colton [155] considered the volatilities were not high enough to support the molecular structures proposed in the early X-ray studies, but these have been substantiated in the later neutron work [14,16].

TABLE 29

The Cl—Cl distances in UCl_6 and β-WCl_6 (Cl—Cl ionic diameter = 3.64 Å)

Compound	Cl—Cl in octahedron (Å)	Other Cl—Cl distances (Å)
UCl_6	3.22—3.63	3.67—4.11
β-WCl_6	3.16—3.56	3.55—3.91
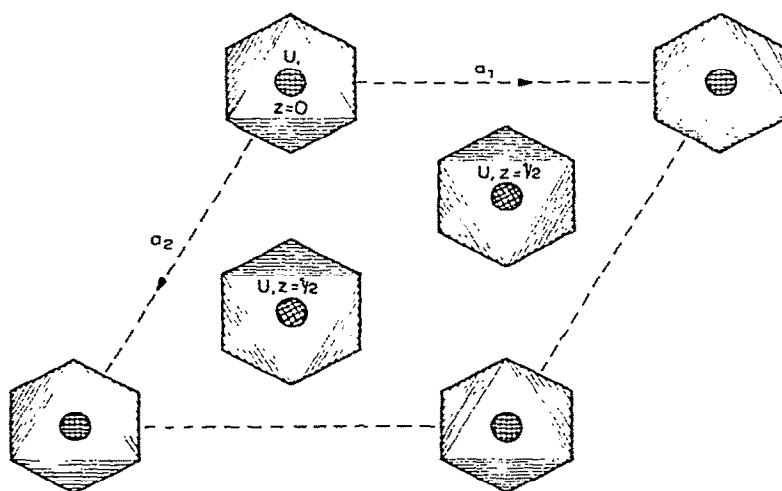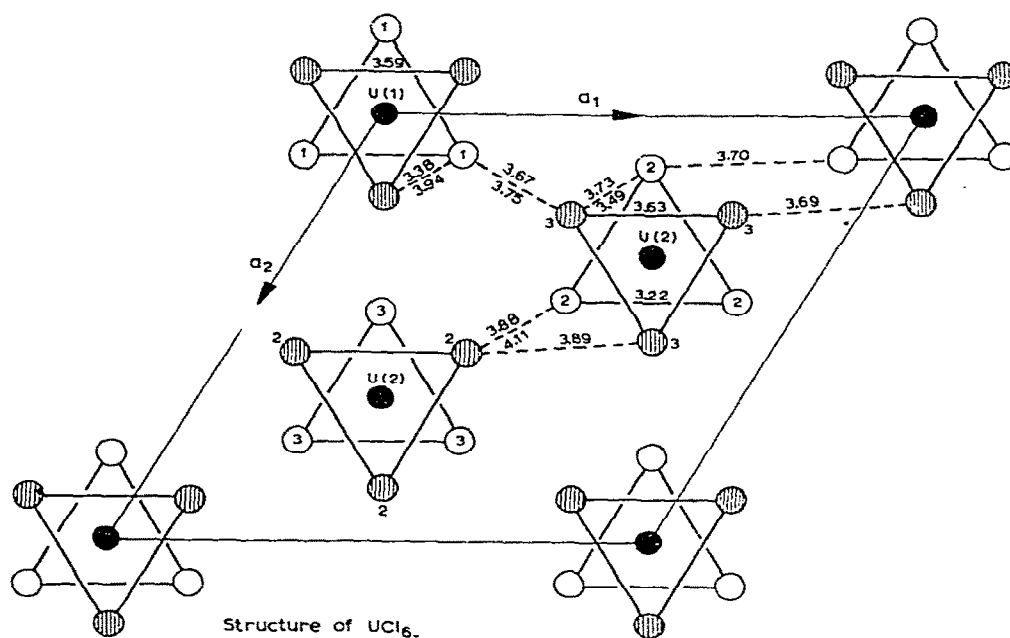
Fig. 37. (a) The crystal structure [14] of UCl_6 showing molecular contact distances. Shaded circles are chlorine atoms near $z = 1/4$, and unshaded circles are chlorine atoms near $z = 3/4$. (b) The UCl_6 structure, illustrating its molecular lattice.

UCl₆

URANIUM HEXACHLORIDE
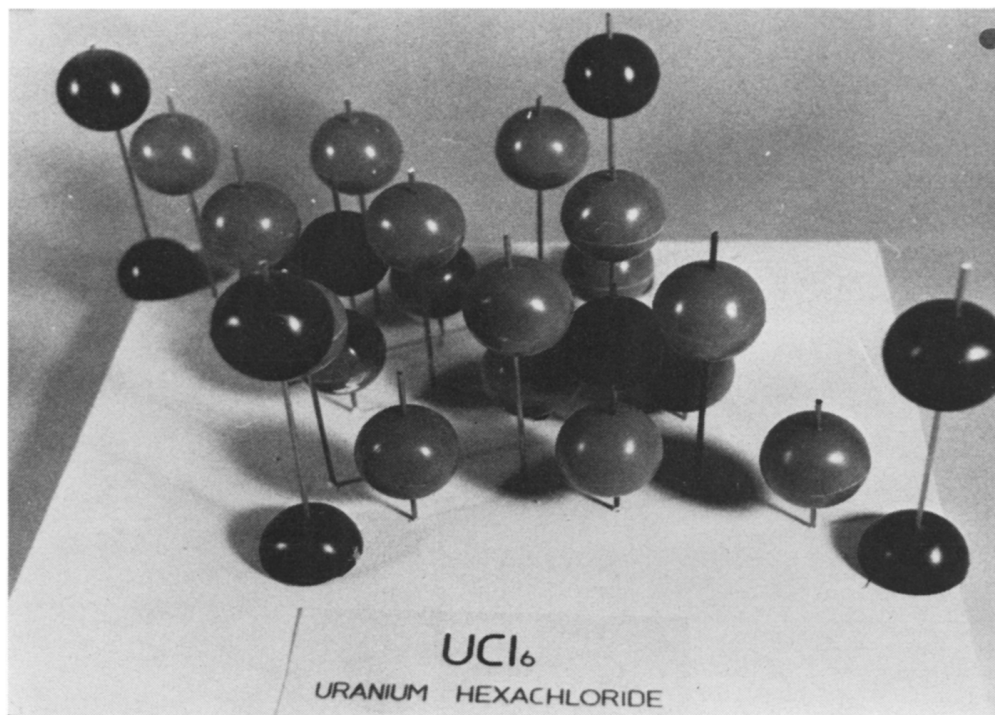
Fig. 38. The atomic arrangement in one unit cell of the UCl_6 structure — perspective view
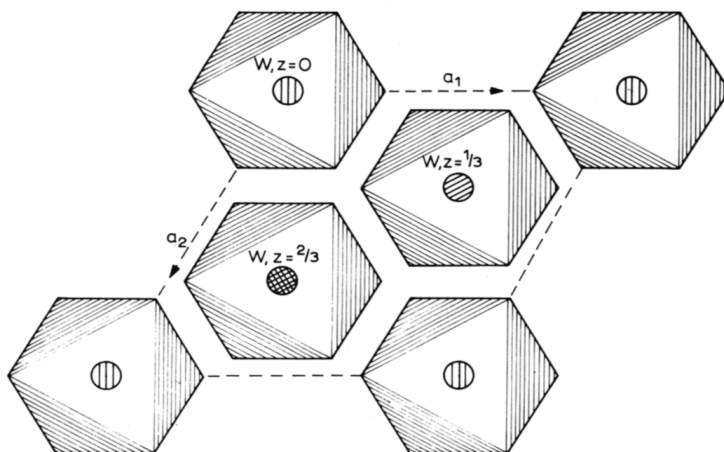
Fig. 39. The α-WCl_6 structure. The h.c.p. layers are the same as in UCl_6, but the arrangement of the metal atoms in octahedral holes is different [154].

H. THE URANIUM OXYHALIDE STRUCTURE TYPES

(i) Trivalent actinide oxyhalide types

AcOF, ThOF, PuOF and CfOF are known [3] but UOF does not appear to have been characterised. The trivalent oxyfluorides are either the 8-coordinate fluorite type or closely related to it. These fluorite-like oxyfluorides occur widely in the lanthanide series and the crystallography of these phases has been reviewed by Brown [2]; the early definitive work was done by Zachariasen [156]. Mann and Bevan [157] recently studied stoichiometric, rhombohedral YOF and interchanged the O and F positions of Zachariasen [156]. Holmberg [158] found ScOF to exist in a monoclinic ZrO_2 type structure [71]. This type is 7-coordinate, with a square base, triangular top polyhedron (see Fig. 2), and is a highly distorted fluorite structure. ZrO_2 transforms to a tetragonal form closely related to fluorite at 1100—1200° and at 2370° to cubic fluorite [159]. Other rare earth oxyfluorides, e.g. $Y_7O_6F_9$, also can have structures closely related to fluorite [160]. Recently, the structures of YSF [161], YSeF

Fig. 40. The infinite $PaOCl_2$ chain in $PaOCl_2$. The configuration around Pa(1) is dodecahedral (C.N. = 8), around Pa(2) a tricapped trigonal prism (C.N. = 9) and around Pa(3) an octahedron + 1 (C.N. = 7). $UOCl_2$ is isostructural with $PaOCl_2$ (after Smith et al. [165]).

TABLE 30

Unit cell data for the isomorphous compounds $ThOCl_2$, $PaOCl_2$, $UOCl_2$ and $NpOCl_2$ (Ref 166)

Compound	a (Å)	b (Å)	c (Å)	Space group
$ThOCl_2$	15.494	18.095	4.018	Pbam
$PaOCl_2$	15.332	17.903	4.012	Pbam
$UOCl_2$	15.255	17.828	3.992	Pbam
$NpOCl_2$	15.209	17.670	3.948	Pbam

[162], SmSI [163] and NdSBr [164] have been reported, but no analogues have been synthesised as yet for uranium or the other actinides.

The trivalent oxyhalide phases MOX with X = Cl, Br, I are known for most of the actinides; all of those studied have the PbFCl structure, with nine halogens arranged around the metal atom in a monocapped square antiprism (Fig. 4 (C.N. = 9)). The crystallographic data for these phases have been tabulated by Brown [3].

(ii) The tetravalent $UOCl_2$ type

The structure of $ThOF_2$, the only reported 4-valent actinide oxy-fluoride, is unknown [3]. With the other halogens, the dominant structure type is the $PaOCl_2$ type [165], whose structure is illustrated in Fig. 40, and contains 7-, 8- and 9-coordinate metal atoms. $ThOCl_2$, $PaOCl_2$, $UOCl_2$ and $NpOCl_2$ and probably the bromides have this structure [166]. $ThOI_2$ [167] and $PaOI_2$ [168

TABLE 31

The known pentavalent oxyhalides [a]

Compound	Pa	U	Np	Pu
MOF_3			√	
$MOCl_3$	?	√		
$MOBr_3$	√	√		
MOI_3	√			
M_2OF_8	√	√		
M_2OCl_8	√			
MO_2F	√	√	√	
MO_2Cl	√	√		?
MO_2Br	√	√		
MO_2I	√			

[a] A blank space in the Table signifies the compound is unknown or unchecked. The question marks mean the existence of $PaOCl_3$ and PuO_2Cl phase is uncertain.

TABLE 32

Unit cell data for PaOBr$_3$ and UOBr$_3$

Compound	a (Å)	b (Å)	c (Å)	β (deg)	Space group
PaOBr$_3$	16.91	3.87	9.33	113.67	C2/m
UOBr$_3$	16.24	3.7	9.0	110.5	C2/m

are known but not structurally characterised. The unit cell data for the oxychlorides (Table 30) shows the isomorphism.

Taylor and Wilson [13] verified the PaOCl$_2$ type for UOCl$_2$ in a neutron powder profile study, and found complete isomorphism; the positional parameters and bond lengths in PaOCl$_2$ [165] and UOCl$_2$ [13] are identical within the experimental errors. Close correspondence occurs because the structures are determined mainly by bridging requirements, and the Pa^{4+} and U^{4+} ionic radii are nearly the same. The backbones of the infinite chains, which are Pa—O and U—O frameworks, resemble the fluorite structure.

The polyhedra around U(1), U(2) and U(3) in UOCl$_2$ are dodecahedral, tricapped trigonal prismatic and octahedral + 1 (see Fig. 4).

(iii) The pentavalent uranium oxyhalide types

The known pentavalent oxyhalides [3,6] are summarised in Table 31.

The only structure type in this area which has been explained is the PaOBr$_3$ type, which was studied by Brown et al. [169,170]. UOBr$_3$ is isostructural [3] with PaOBr$_3$ as shown by the cell dimensions in Table 32. The PaOBr$_3$ structure is made up of the double endless chains, shown in Fig. 41. The chains pack into the structure as shown in Fig. 42. The polyhedra in the chains are pentagonal bipyramids, which are highly condensed, four of the five pentagonal edges being shared with other polyhedra. The chains are not quite endless; occasional random terminations appear to cause structural disorder and limit the quality of the diffraction data. Of the structure and structure type however, there is no doubt. The double chain also occurs in the nonstoichiometric compound [171] Cs$_{0.9}$UO$_3$Cl$_{0.9}$, and the chlorine shortfall here could also be due to chain terminations.

The (UO$_2$Cl, UO$_2$Br) structure [172] is unknown. Bagnall [4] has suggested possible structures for U$_2$OF$_8$ and Pa$_2$OF$_8$.

(iv) The hexavalent uranium oxyhalide types

The presently known phases of the hexavalent uranium oxyhalide types are shown in Table 33.
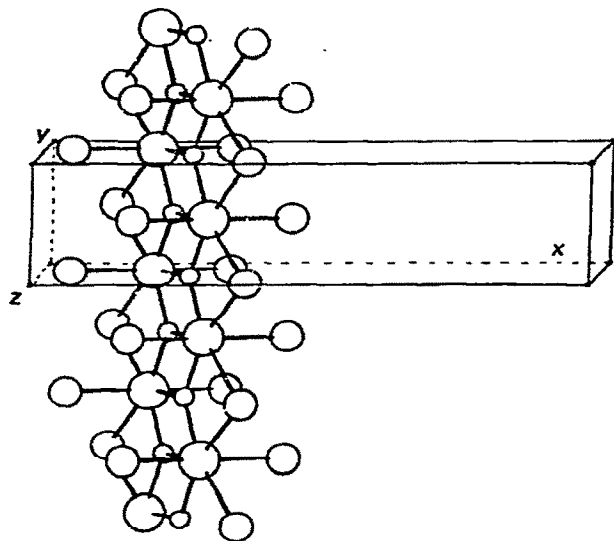
Fig. 41. The endless double chains which form the PaOBr₃ structure (after Brown et al. [170]).

(a) Uranyl fluoride

In uranyl fluoride, UO_2F_2, six fluorine atoms can be accommodated around the small but highly charged linear uranyl ion in its equatorial plane to form a structure type unique to the actinides [173]. The C.N. value 8 is high for hexavalent uranium. Recently, neutron diffraction studies [174,175] have shown that the equatorial fluorine hexagon is only slightly puckered, with U—O distances of 1.74(2) Å and U—F = 2.429(2) Å. Thus Zachariasen's original diagram [173], which shows a puckering of ±0.61 Å and a U—O distance of 1.91 Å determined from packing considerations, needs modification although his structure is essentially correct. The structure is completely layered,
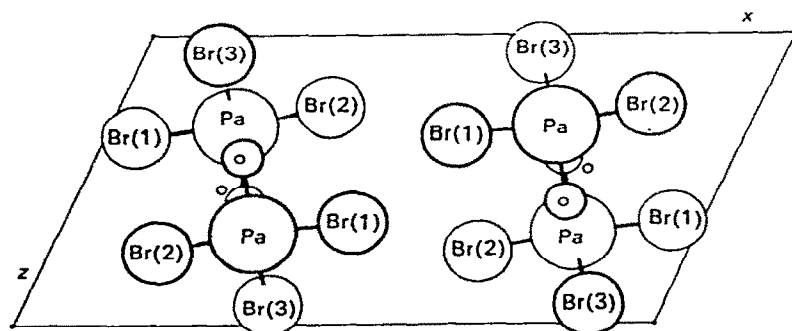
Fig. 42. The packing of the endless PaOBr₃ double chains in the crystal structure (after Brown et al. [170]).

TABLE 33

The known hexavalent actinide oxyhalides [a]

Compound	U	Np	Pu	Am
MO_2F_2	√	√	√	√
MO_2Cl_2	√		√ [b]	
MO_2Br_2	√			
MO_2I_2	?			
MOF_4	√			
$M_2O_3F_6$	√			
$M_3O_5F_8$	√			

[a] Blank spaces mean the compound is unchecked or unknown.
[b] As hexahydrate.

the fluorine hexagons being fused on all edges (Fig. 43) and the layers are bonded by van der Waals' forces. The high symmetry of the layers leads to frequent stacking faults which make certain classes of reflexions diffuse. Electron micrographs [174] show needle-like particles which could be capable of causing further broadening effects. NpO_2F_2 [176], PuO_2F_2 [177] and AmO_2F_2 [178] are isostructural with UO_2F_2 as shown by the cell dimensions (Table 34).

(b) Uranyl fluoride—alkali fluoride—H_2O complexes
These phases are all based on pentagonal bipyramids (with apical uranyl oxygens, and water oxygen or fluorine in the equatorial pentagon) in various

Fig. 43. The uranyl fluoride strutcure (after Taylor and Wilson [174]).

TABLE 34

Unit cell dimensions for UO_2F_2, NpO_2F_2, PuO_2F_2 and AmO_2F_2 (hexagonal axes)

	a	c	Space group	Ref.
UO_2F_2	4.192	15.66	$R\bar{3}m$	174
NpO_2F_2	4.185	15.79	$R\bar{3}m$	176
PuO_2F_2	4.154	15.81	$R\bar{3}m$	177
AmO_2F_2 ·	4.136	15.85	$R\bar{3}m$	178

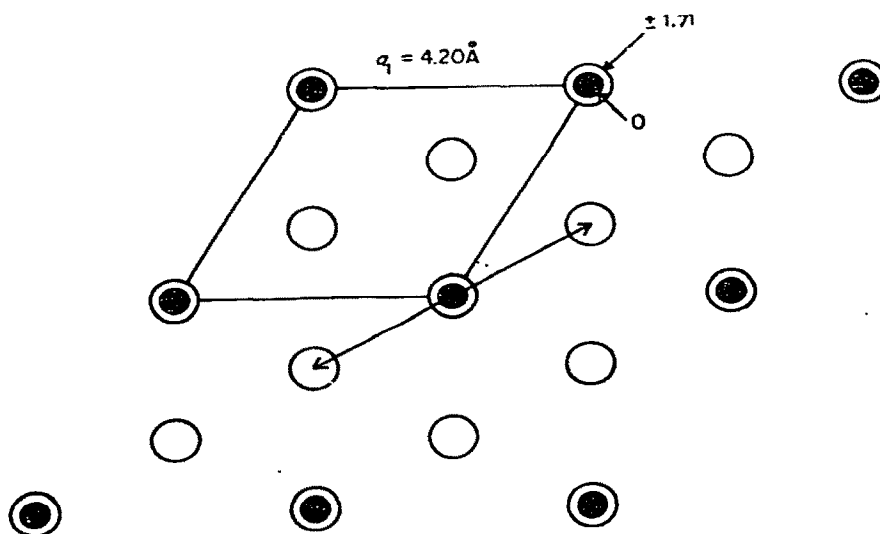states of polyhedral polymerisation. The complexes whose structures have been determined are listed in Table 35, together with the crystal data. The structure types are shown as A → E.

The structure types A → E are illustrated in Fig. 44. Type A consists of M^+ and $UO_2F_5^{3-}$ ions, type B has edge-fused dimers $(UO_2)_2F_8^{4-}$, type C has corner-fused dimers $(UO_2)_2F_9^{5-}$, type D has dimers $(UO_2)_2(O_{aq})_2F_6^{2-}$, and finally type E the endless chains $[(UO_2)_2F_7^{3-}]_\infty$.

(c) Uranium oxide tetrafluoride

Strangely, this important compound was only characterised recently by Wilson [27], who synthesised UOF_4 by reacting UF_6 with a dilute solution of H_2O in HF. Paine et al. [28] prepared single crystals of UOF_4 by controlled hydrolysis according to the reaction:

$$2\,UF_6 + SiO_2 \xrightarrow[HF(\ell)]{} 2\,UOF_4 + SiF_4$$
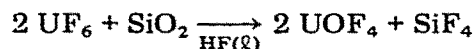
TABLE 35

Crystal data for uranyl fluoride—alkali fluoride complexes

Compound	Ref.	a (Å)	b (Å)	c (Å)	β (deg)	Space group	Structure type [a]
$K_3UO_2F_5$	179	9.16		18.17		$I4_1/a$	A
$Rb_3UO_2F_5$	180	9.53		18.57		$I4_1/a$	A
$(NH_4)_3UO_2F_5$	181	29.22	9.48	13.51	136.1	Cm	A
$Rb_2UO_2F_4 \cdot H_2O$	182	8.88	14.55	11.98		Pbca	B
$Cs_2UO_2F_4 \cdot H_2O$	183	8.06	12.18	9.29	109.2	$P2_1/c$	B
$K_5(UO_2)_2F_9$	184	19.86	6.11	11.71	102.6	C2/c	C
$CsUO_2F_3 \cdot H_2O$	185	9.45	11.54	6.04	95.5	$P2_1/a$	D
$K_3(UO_2)_2F_7 \cdot 2\,H_2O$	186	6.23	9.31	11.60	94.4	P2/m	E

[a] The structure types A → E are illustrated in Fig. 44. Type A consists of M+ and $UO_2F_5^{3-}$ ions; type B has edge-fused dimers $(UO_2)_2F_8^{4-}$; type C has corner-fused dimers $(UO_2)_2F_9^{5-}$; · type D has dimers $(UO_2)_2(O_{aq})_2F_6^{2-}$; and finally, type E the endless chains $[(UO_2)_2F_7^{3-}]_\infty$.
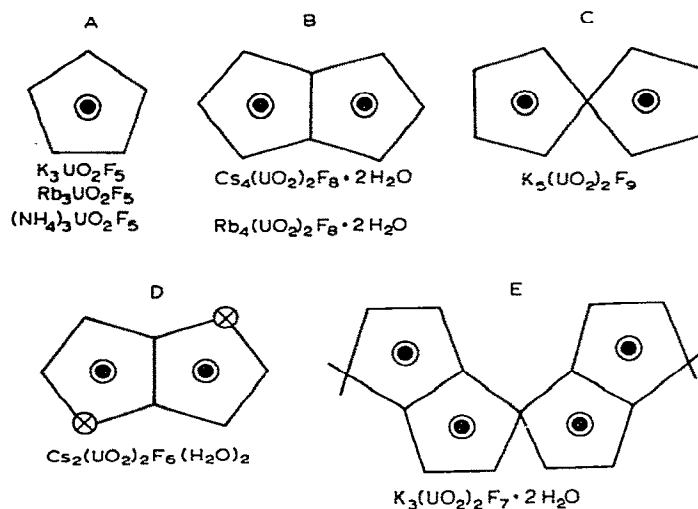
Fig. 44. Structure types found in the uranyl fluoride—alkali fluoride—water complexes: A, $K_3UO_2F_5$ type; B, $Rb_4(UO_2)_2F_8 \cdot 2 H_2O$ type; C, $K_5(UO_2)_2F_9$ type; D, $Cs_2(UO_2)_2F_6(H_2O)_2$ type; E, $K_3(UO_2)_2F_7 \cdot 2 H_2O$ type.

The two preparations gave the same X-ray pattern, and the phase is denoted as α-UOF$_4$. A second form of UOF$_4$, β-UOF$_4$, was observed [29] to grow slowly on the walls of a Kel-F tube over a slurry of α-UOF$_4$ in HF. β-UOF$_4$ gives an IR spectrum identical to that of α-UOF$_4$, and a powder pattern similar to that of β-UF$_5$. The IR spectrum showed the crystals were not UF$_5$. The isomorphism was apparently possible because of the similar sizes of oxygen and fluorine (cf. the isomorphism of WOF$_4$ and WF$_5$ and the similarity of MoOF$_4$, α-TcOF$_4$ and ReOF$_4$ with the VF$_5$ types, Table 20). Polymorphism is not uncommon in the oxyhalides, being found in TcOF$_4$, MoOF$_4$ and CrOF$_4$. Crystal data for α-UOF$_4$, β-UOF$_4$ and β-UF$_5$ are given in Table 36.

The structure of α-UOF$_4$ was determined by Paine et al. [28] by single-crystal X-ray diffraction, and is shown in Fig. 45. It contains pentagonal bi-

TABLE 36

Crystal data for α-UOF$_4$, β-UOF$_4$ and β-UF$_5$

Compound	a (Å)	c (Å)	Space group	Ref.
α-UOF$_4$	13.22	5.72 [a]	R3m	28
β-UOF$_4$	11.4743	5.2043	I42d	31
β-UF$_5$	11.473	5.209	I42d	60

[a] Triple hexagonal cell.
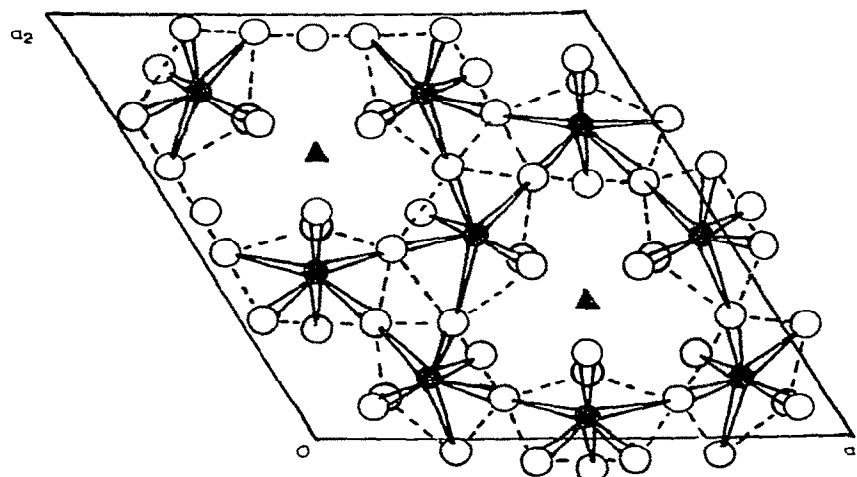
Structure of α-UOF₄

Fig. 45. The structure [28,187] of α-UOF₄, showing the pentagonal bipyramids corner-fused in rhombohedral fashion into a 3-dimensional network. The equivalent triple hexagonal cell is drawn (after Paine et al. [28] and Levy et al. [187]).

pyramids, corner linked into a rhombohedral, 3-dimensional framework. It is difficult to distinguish oxygen from fluorine with this technique, but the oxygen density was considered to be in the axial positions (U—X (axial) ∼ 1.78 Å). The non-bridging equatorial fluorine atom was 1.98 Å from uranium, and the four bridging fluorine atoms were 2.25—2.29 Å from the uranium atom. The extensive 3-D bridge network explains the surprisingly low volatility of the compound, as compared with UF_6. A neutron diffraction study of α-UOF₄ has now been completed [187] and is more precise than the X-ray study. It shows terminal bonds whose lengths are the average of the expected U—O and U—F distances, suggesting O, F disorder in the terminal positions.

The structure of β-UOF₄, also determined by single-crystal X-ray analysis [30,31], is shown in Fig. 13. The pentagonal bipyramidal polyhedra are corner-shared in the equatorial positions as in α-UOF₄, but they link differently, to give a tetragonal structure of the β-UF₅ type [60], which is still highly three-dimensionally bridged. As in α-UOF₄, the terminal bonds are shorter than the bridging bonds. The oxygen density was assumed to reside mainly in the terminal ring position, with the possibility of some O, F disorder (and thus partial oxygen density) in the axial positions. No oxygen density was considered to occur in the bridge bonds. Some evidence for O, F disorder lay in the high thermal parameters of the terminal atoms, for which there was also some evidence in the thermal parameters for α-UOF₄. O, F disorder has to be assumed in WOF₄, to account for the terminal multiple W—O bonds indicated by the IR and Raman spectra [188]. The crystal symmetry requires the oxygen atoms

TABLE 37

Crystal data for anhydrous UO_2Cl_2, $UO_2Cl_2 \cdot H_2O$ and $UO_2Cl_2 \cdot D_2O$

Compound	a (Å)	b (Å)	c (Å)	β (deg)	Space group	Ref.
UO_2Cl_2	5.725	8.409	8.720		Pnma	191, 16
$UO_2Cl_2 \cdot H_2O$	5.836	8.563	5.566	97.70	$P2_1/m$	191, 17
$UO_2Cl_2 \cdot D_2O$	5.847	8.596	5.543	97.51	$P2_1/m$	17

in WOF_4 to be in the bridge positions of the tetramer for an ordered structure.

A comparison of Figs. 45 and 13, and comparison of the volumes per molecule and density of α- and β-UOF_4 show that β-UOF_4 is the more dense phase (ρ_c = 6.40 gm cm^{-3} for β-UOF_4 and 5.7 gm cm^{-3} for α-UOF_4; volume per molecule = 85.7 Å^3 in β-UOF_4 and 96.2 Å^3 in α-UOF_4). It is logical that the slowly formed crystals should have the higher density.

(d) Other uranium(VI) oxyfluorides

The oxyfluorides $U_2O_3F_6$ and $U_3O_5F_8$ have been reported [189] but are not characterised structurally. $CaU_2O_6F_2$ is an isotype of U_3O_8 [190].

Fig. 46. The crystal structure of anhydrous UO_2Cl_2 seen down a. The U atoms are solid circles, Cl atoms shaded circles and O atoms open circles. The x-coordinates are indicated (after Taylor and Wilson [16]).

(v) Uranyl chloride and its hydrates

Uranyl chloride, UO_2Cl_2, is the only known dioxodichloride in the actinide series except for hydrated PuO_2Cl_2, and the only actinide dioxodihalide to be characterised structurally. Uranyl chloride and its hydrates were the subject of an X-ray powder study by Debets [191], in which the oxygen locations could only be determined with low accuracy. The crystal data for UO_2Cl_2 and its mono-hydrate and monodeuterate are given in Table 37. The structures of UO_2Cl_2, $UO_2Cl_2 \cdot H_2O$ and $UO_2Cl_2 \cdot D_2O$ have been determined in neutron powder pro-file studies by Taylor and Wilson [16,17]. The neutron study [16] showed that the X-ray positions for the oxygen atoms needed modification in anhy-drous UO_2Cl_2, whose structure is shown in Fig. 46. The polyhedron around uranium is a pentagonal bipyramid, and the pentagonal rings share edges to form endless chains parallel to b; these chains are cross linked by one of the oxygens, O(1), which is an apical atom in one bipyramid and a pentagonal
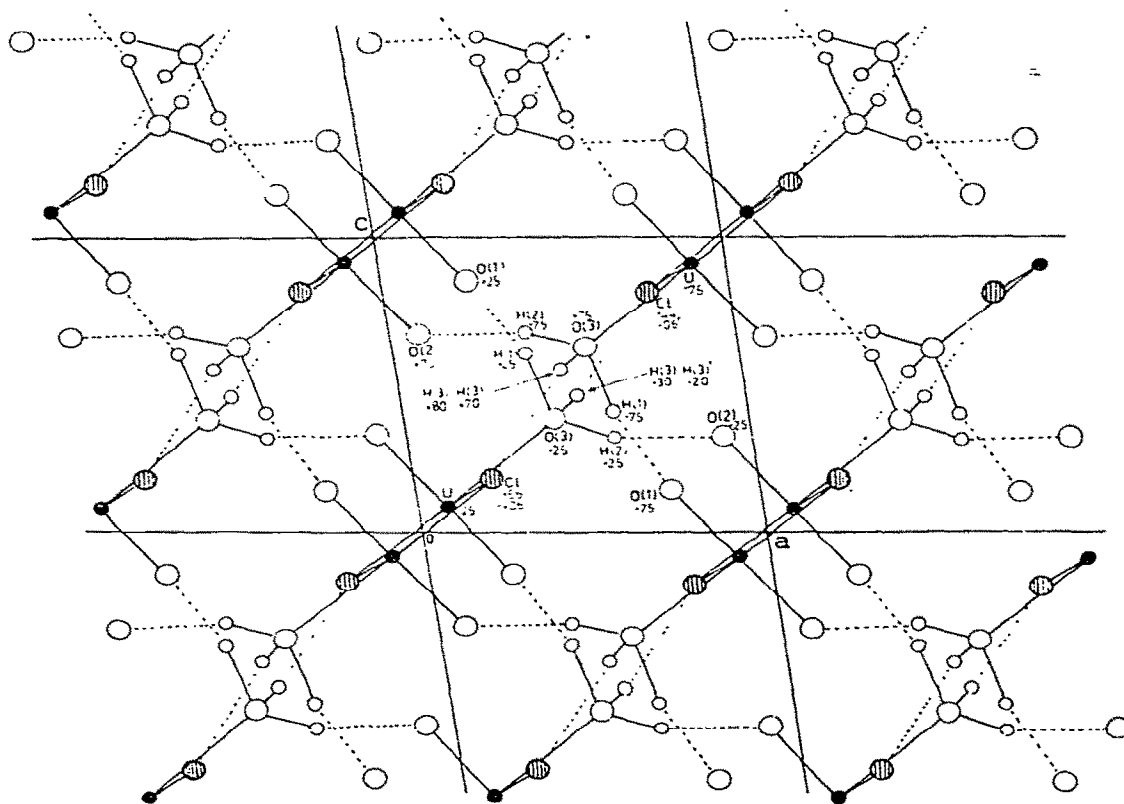

Fig. 47. The structure of $UO_2Cl_2 \cdot H_2O$ (and $UO_2Cl_2 \cdot D_2O$) as viewed down the unique b-axis. Some y-coordinates are shown (after Taylor and Wilson [17]).

ring oxygen in the adjacent bipyramid. Thus, the U—O(1) bond, 1.78(2) Å is slightly longer than the U—O(2) bond, which is terminal and closer to the true uranyl distance, 1.71 Å. The UO_2Cl_2 structure is completely different from the UO_2F_2 structure because of the different size of the anions; six chlorine atoms cannot be fitted around the equator of the uranyl group. The formula for UO_2Cl_2 is $[UOO_{2/2}Cl_{4/2}]$ and for UO_2F_2 is $[UO_2F_{6/3}]$. The UO_2Cl_2 structure is reminiscent of the UBr_4 structure (Sect. E(iv)) but although a dual-purpose atoms links the chains in both compounds, the bridges in UO_2Cl_2 are single and linear and in UBr_4 doubled, resulting in a 3-dimensional network in UO_2Cl_2 and a layer structure in UBr_4.

Uranyl chloride monohydrate is monoclinic (Table 37). Debets' X-ray positions for oxygen led to anomalous bond distances and he concluded that the compound could not be a true hydrate. The neutron powder profile study of the hydrate and deuterate [17] led to revision of the oxygen positions and gave normal bond distances. The water molecules, however, were in two-fold positional disorder. Statistical half-hydrogens (or half-deuteriums) completed hydrogen bonds with both uranyl oxygens (terminal) and chlorine atoms. The $UO_2Cl_2 \cdot H_2O$ structure is shown in Figs. 47 and 48. The fused pentagonal chains again occur, but the uranyl oxygens are terminal and the water oxygen
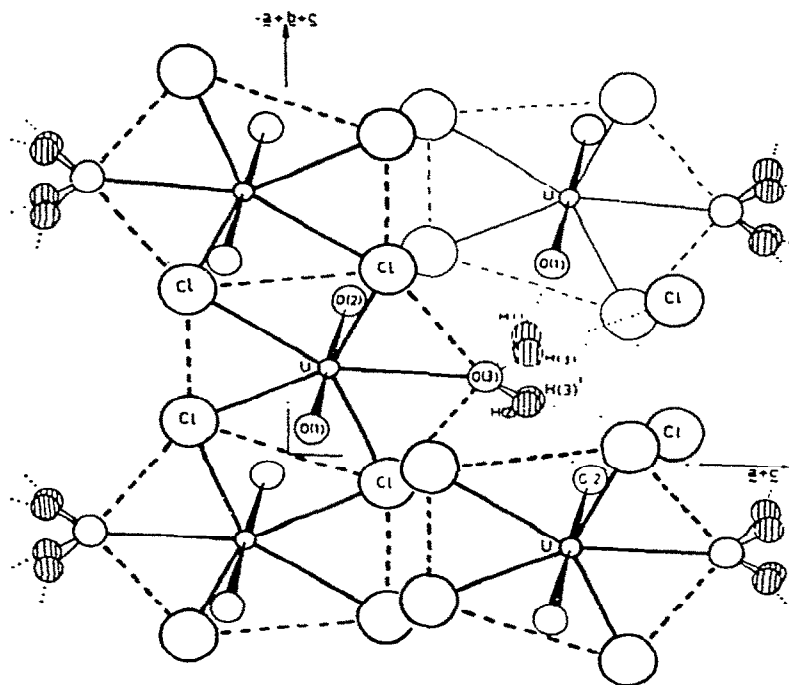

Fig. 48. The structure of $UO_2Cl_2 \cdot H_2O$ (and $UO_2Cl_2 \cdot D_2O$) projected down an axis $a + b$ — c, showing the pentagonal chains and the proton (or deuteron) disorder (after Taylor and Wilson [17]).
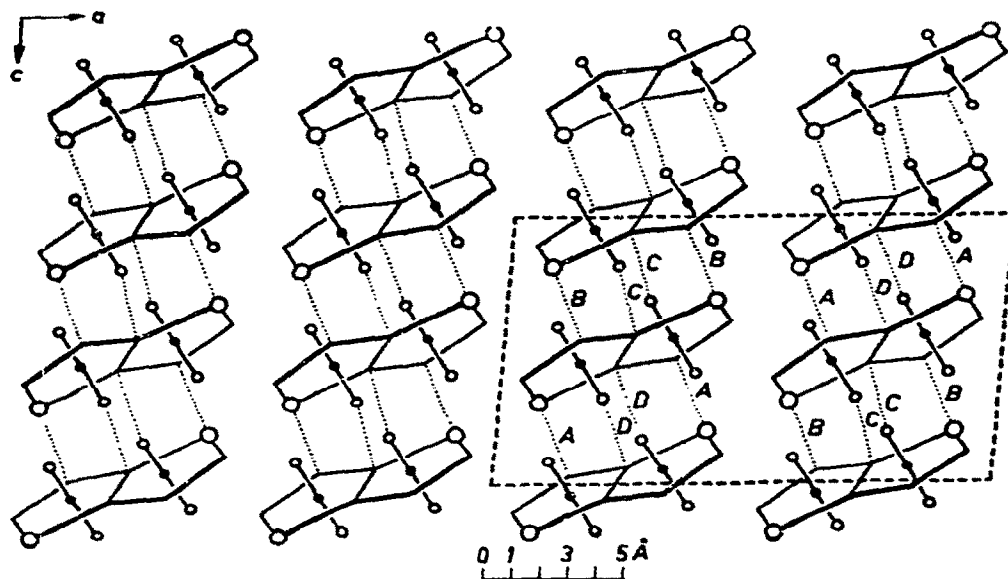
Fig. 49. The crystal structure of the basic uranyl chloride hydrate [(UO$_2$)$_2$Cl$_2$(OH)$_2$ (H$_2$O)$_4$] (after Aberg [192]).

is part of the pentagonal ring. The chains are held together in the crystal through the hydrogen bonds. The structural formula is [UO$_2$Cl$_{4/2}$OH$_2$]$_\infty$.

A structure for uranyl chloride trihydrate has been proposed [191] and needs confirmation by neutron diffraction. The crystal structure of the basic uranyl chloride hydrate [(UO$_2$)$_2$Cl$_2$(OH)$_2$ · (H$_2$O)$_4$] has been determined [192] and is shown in Fig. 49. The dimeric molecules are held in the crystal by hy-
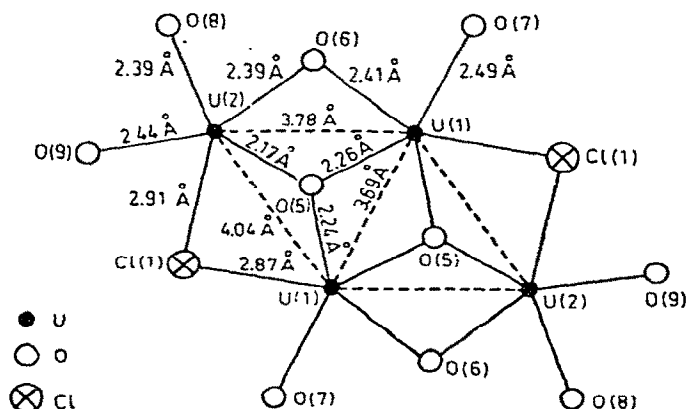

Fig. 50. The crystal structure of the basic uranyl chloride hydrate [(UO$_2$)$_4$O$_2$(OH)$_2$-Cl$_2$(H$_2$O)$_6$] (after Aberg [193]).
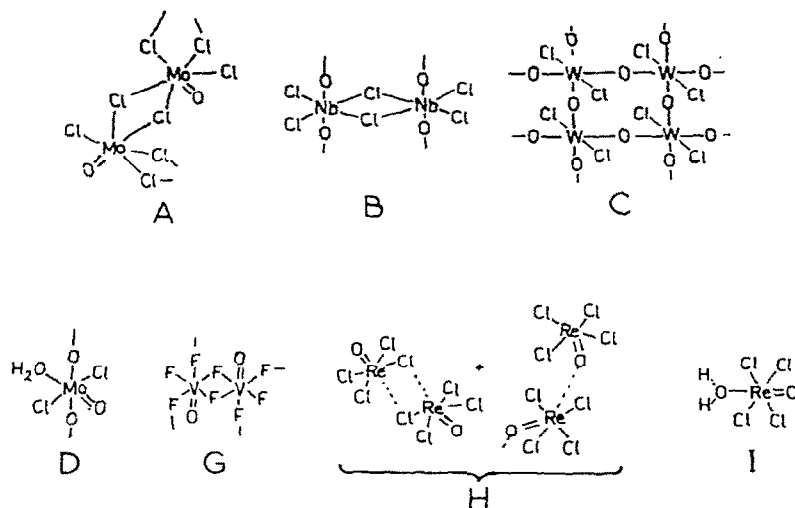
Fig. 51. Some transition metal oxyhalide structure types. A, High-MoOCl$_3$ [194,195], TcOCl$_3$ [194], ReOBr$_3$ [194]; B, NbOCl$_3$ [196], low-MoOCl$_3$ [195], WOCl$_3$ [194], WOBr$_3$ [74], MoOBr$_3$ [194], TcOBr$_3$ [74], NbOBr$_3$ [194], TaOCl$_3$ [107]; C, MoO$_2$Br$_2$ [197], WO$_2$Cl$_2$ [198], WO$_2$Br$_2$ [197], MoO$_2$Cl$_2$ [199], WO$_2$I$_2$ [200]; D, MoO$_2$Cl$_2 \cdot$ H$_2$O [201]; E, ReOF$_4$ [132], MoOF$_4$ [130]; F, WOF$_4$ [125]; G, VOF$_3$ [202], CrO$_2$F$_2$ [202], VF$_4$ [202]; H, ReOCl$_4$ [203]; I, ReOCl$_4 \cdot$ H$_2$O [204].

drogen bonds and, once again, pentagonal bipyramids are found. [(UO$_2$)$_4$O$_2$-(OH)$_2$Cl$_2$(H$_2$O)$_6$] has a tetrameric structure (Fig. 50) based on the pentagonal bipyramid [193]. All the pentagon atoms are co-planar in the tetramer.

(vi) A brief comparison of the uranium and transition metal oxyhalides

WOCl$_4$ and WOBr$_4$ are the only transition metal oxyhalides known to conform to an actinide halide structure type. The transition metal oxyhalide types so far discovered are based on octahedra, sometimes distorted to square pyramidal dimers (Fig. 51 H). Some of the many structure types encountered in the transition metal oxyhalides are shown in Fig. 51. The main reason why the C.N. generally does not rise above 6 in the transition metal series, whereas it most commonly does so in the actinide series, is the cation size effect.

L. CONCLUSIONS

Uranium shows a bewildering variety of structure types and anion polyhedra in its halide and oxyhalide compounds. This is due to three main factors

the range of uranium and anion sizes;
the availability of f as well as d-orbitals for bonding;
and the oxidation state range of 3—6.

The uranium halide and oxyhalide structure types persist along the actinide series, transitions occurring when the actinide contraction requires another structure type of smaller C.N. Where the sizes and valence of uranium and the transition metals are comparable, the uranium types also are found in the transition metal and lanthanide binary halides, e.g. UF_6 and MoF_6, $\cdots$, UF_4 and α-ZrF_4, UF_3 and LaF_3, $\cdots$, UCl_3 and $LaCl_3$, $\cdots$, $UOCl$ and $LaOCl$, $\cdots$. This may indicate that size effects dominate covalent bonding effects. Most uranium oxyhalide structure types are not generally found in the lanthanides and actinides, because either (a) they are very complicated, e.g. $UOCl_2$, and differences in electronic configuration may force different structures in the other series or (b) in the hexavalent case, the linear uranyl group with its short multiple bonds to both oxygens does not have a counterpart in the other series.

In the binary halides, as the oxidation state increases and the uranium size decreases, the halogen bridges decrease in number and the compounds tend to become more molecular with some covalent character in the bonds. This trend leads to marked changes in physical properties such as volatility and melting point, as noted in the $UF_3 \rightarrow UF_6$ series. The anion polyhedra generally tend to conform to the theoretical polyhedra, any distortions being explicable in terms of bridging requirements or coulombic repulsions. Polymorphism is very common, for with the large cations and high C.N., the energetic differences between alternative polyhedra are small. Sometimes, as in the case of $ThCl_4$ and UCl_5, the polyhedra remain of the same type, but pack more efficiently in a low-temperature form.

J. ACKNOWLEDGEMENTS

K. REFERENCES

1 D. Brown, in K.W. Bagnall (Ed.), International Review of Science, Vol. 7, M.T.P. and Butterworths, London, 1972, Chap. 3.
2 D. Brown, Halides of the Lanthanides and Actinides, Wiley, New York, 1968.
3 D. Brown, in J.C. Bailar et al. (Eds.), Comprehensive Inorganic Chemistry, Vol. 5, Pergamon Press, Oxford, 1973, p. 151.
4 K.W. Bagnall, The Actinide Elements, Elsevier, Amsterdam, 1972.
5 K.W. Bagnall, in V. Gutmann (Ed.), Halogen Chemistry, Vol. 3, Academic Press, London, 1967, Chap. 7.
6 C. Keller, The Chemistry of the Transuranium Elements, Verlag Chemie, Weinheim, 1971.
7 R.A. Penneman, R.R. Ryan and A. Rosenzweig, Struct. Bonding (Berlin), 13 (1973) 1.

8 P.T. Moseley, M.T.P. Int. Rev. Sci., Ser. 2, 7 (1975) 65.
9 J.C. Taylor and P.W. Wilson, Acta Crystallogr., Sect. B, 30 (1974) 2803.
10 J.H. Levy, J.C. Taylor and P.W. Wilson, J. Less Common Metals, 39 (1975) 265.
11 J.H. Levy, J.C. Taylor and P.W. Wilson, Acta Crystallogr., Sect. B, 31 (1975) 880.
12 J.C. Taylor and P.W. Wilson, Acta Crystallogr., Sect. B, 29 (1973) 1942.
13 J.C. Taylor and P.W. Wilson, Acta Crystallogr., Sect. B, 30 (1974) 175.
14 J.C. Taylor and P.W. Wilson, Acta Crystallogr., Sect. B, 30 (1974) 1481.
15 J.C. Taylor and P.W. Wilson, Acta Crystallogr., Sect. B, 30 (1974) 1216.
16 J.C. Taylor and P.W. Wilson, Acta Crystallogr., Sect. B, 29 (1973) 1073.
17 J.C. Taylor and P.W. Wilson, Acta Crystallogr., Sect. B, 30 (1974) 169.
18 J.C. Taylor, P.W. Wilson and J.W. Kelly, Acta Crystallogr., Sect. B, 29 (1973) 7.
19 J.C. Taylor and P.W. Wilson, J. Solid State Chem., 14 (1975) 378.
20 J.H. Levy, J.C. Taylor and P.W. Wilson, J. Chem. Soc., Dalton Trans., (1976) 219.
21 J.H. Levy, J.C. Taylor and P.W. Wilson, Acta Crystallogr., Sect. B, 31 (1975) 398.
22 J.H. Levy, P.L. Sanger, J.C. Taylor and P.W. Wilson, Acta Crystallogr., Sect. B, 31 (1975) 1065.
23 J.H. Levy, J.C. Taylor and P.W. Wilson, J. Solid State Chem., 15 (1975) 360.
24 J.H. Levy, J.C. Taylor and P.W. Wilson, J. Less Common Metals, 45 (1976) 155.
25 J.C. Taylor and P.W. Wilson, Chem. Commun., (1974) 598.
26 J.C. Taylor and P.W. Wilson, Acta Crystallogr., Sect. B, 30 (1974) 2664.
27 P.W. Wilson, J. Inorg. Nucl. Chem., 36 (1973) 303.
28 R.T. Paine, R.R. Ryan and L.B. Asprey, Inorg. Chem., 14 (1975) 1113.
29 J.C. Taylor and P.W. Wilson, Chem. Commun., (1974) 232.
30 J.C. Taylor and P.W. Wilson, Acta Crystallogr., Sect. B, 30 (1974) 1701.
31 U. Müller and W. Kolitsch, Z. Anorg. Allg. Chem., 410 (1974) 32.
32 J.T. Mason, M.C. Jha and P. Chiotti, J. Less Common Metals, 34 (1974) 143.
33 J.T. Mason, M.C. Jha, D.M. Bailey and P. Chiotti, J. Less Common Metals, 35 (1974) 331.
34 R.D. Baybarz, J. Inorg. Nucl. Chem., 35 (1973) 483.
35 R.D. Baybarz, L.B. Asprey, C.E. Strouse and E. Fukushima, J. Inorg. Nucl. Chem., 34 (1972) 3427.
36 R.D. Shannon and C.T. Prewitt, Acta Crystallogr., Sect. B, 25 (1969) 925.
37 L. Pauling, Nature of the Chemical Bond, 3rd edn., Cornell University Press, New York, 1960, p. 524.
38 A.J. Smith, 10th Int. Congr. Crystallogr., Collect. Abstr., Acta Crystallogr., Sect. A, 31, Part S3 (1975), S146.
39 A. Kitaigorodskii, 10th Int. Congr. Crystallogr., Conference Lecture, Amsterdam, 7—15 August 1975.
40 R.B. King, J. Am. Chem. Soc., 92 (1970) 6455.
41 J.J. Katz and G.T. Seaborg, The Chemistry of the Actinide Elements, Methuen, London, 1957, p. 465.
42 W.H. Zachariasen, Acta Crystallogr., 2 (1949) 390.
43 E.L. Muetterties and C.M. Wright, Q. Rev., Chem. Soc., 21 (1967) 109.
44 W.H. Zachariasen, Acta Crystallogr., 2 (1949) 388.
45 K. Schlyter, Ark. Kemi, 5 (1953) 73.
46 R.W.G. Wyckoff, Crystal Structures, Vol. 2., Wiley, New York, 1964.
47 I. Oftedal, Z. Phys. Chem., Abt. B, 13 (1931) 190.
48 A. Zalkin, D.H. Templeton and T.E. Hopkins, Inorg. Chem., 5 (1966) 1466.
49 J. Laveissiere, Bull. Soc. Fr. Mineral. Cristallogr., 110 (1967) 304.
50 M. Mansmann, Z. Kristallogr., 122 (1965) 375.
51 C. de Rango, G. Tsoucaris and C. Zelwer, C.R. Acad. Sci., 263C (1966) 64.
52 M. Mansmann and W.E. Wallace, J. Phys. (Paris), 25 (1964) 454.
53 C. Choi, New Phys. (Korea), 7 (1967) 37.
54 A.C. Larson, R.B. Roof, Jr. and D.T. Cromer, Acta Crystallogr., 17 (1964) 555.

55 R.D. Burbank and F.N. Bensey, Jr., USAEC Report K-1280 (1956).

56 A.A. Deribas, E.D. Ruchkin, V.S. Filatkina and L.A. Khripin, Fiz. Goreniya Vzryva, (1966) 143.

57 J. Laveissiere, Bull. Soc. Fr. Mineral. Cristallogr., 110 (1967) 308.

58 G. Brunton, Acta Crystallogr., Sect. B, 25 (1969) 1919.

59 A. Rosenzweig, R.R. Ryan and D.T. Cromer, Acta Crystallogr., Sect. B, 29 (1973) 460.

60 W.H. Zachariasen, Acta Crystallogr., 2 (1949) 296.

61 J. Fischer and E. Rudzitis, J. Am. Chem. Soc., 81 (1959) 6375.

62 H. Hess and H. Hartung, Z. Anorg. allg. Chem., 344 (1966) 157.

63 L. Stein, Inorg. Chem., 3 (1964) 995.

64 J.L. Hoard and J.D. Stroupe, USAEC Report TID-5290, Book 1, Paper 45, (1958).

65 R.J. Ackermann and E.G. Rauh, J. Inorg. Nucl. Chem., 35 (1973) 3787.

66 L. Eyring, in A.M. Alper (Ed.), High Temperature Oxides, Academic Press, New York, (1970), Chap. 2, pp. 42, 66.

67 K. Sahl and J. Zemann, Naturwissenschaften, 48 (1961) 641.

68 A.F. Wells, Structural Inorganic Chemistry, 3rd edn., Oxford University Press, 1962, p. 338.

69 H. Barnighausen, H.P. Beck and H.W. Grueniger, 9th Rare Earth Conference, Blacksburg, Virginia, CONF-711001, (1971) p. 74.

70 H. Barnighausen and N. Schultz, Acta Crystallogr., Sect. B, 25 (1969) 1104.

71 J.D. McCullough and K.N. Trueblood, Acta Crystallogr., 12 (1959) 507.

72 L.J. Guggenberger and R.A. Jacobsen, Inorg. Chem., 7 (1968) 2257.

73 J.R. Peterson and B.B. Cunningham, J. Inorg. Nucl. Chem., 30 (1968) 1775.

74 J.N. Stevenson and J.R. Peterson, J. Inorg. Nucl. Chem., 35 (1973) 3481.

75 R.E. Thoma and G.D. Brunton, Inorg. Chem., 5 (1966) 1937.

76 J.H. Burns, J.R. Peterson and J.N. Stevenson, J. Inorg. Nucl. Chem., 37 (1975) 743.

77 A.K. Cheetham and N. Norman, Acta Chem. Scand., Ser. A, 28 (1974) 55.

78 A. Zalkin and D.H. Templeton, J. Am. Chem. Soc., 75 (1953) 2453.

79 W.H. Zachariasen, Acta Crystallogr., 1 (1948) 265.

80 D. Brown and J. Edwards, J. Chem. Soc., Dalton Trans., (1972) 1757.

81 J.H. Levy and J.C. Taylor, unpublished observations, 1976.

82 J.H. Burns and J.R. Peterson, Acta Crystallogr., Sect. B, 26 (1970) 1885.

83 J.R. Peterson and J.H. Burns, J. Inorg. Nucl. Chem., 35 (1973) 1525.

84 J.H. Burns, J.R. Peterson and R.D. Baybarz, J. Inorg. Nucl. Chem., 35 (1973) 1171.

85 L.B. Asprey, T.K. Keenan and F.H. Kruse, Inorg. Chem., 4 (1965) 985.

86 B. Morosin, J. Chem. Phys., 49 (1968) 3007.

87 B. Morosin and A. Narath, J. Chem. Phys., 40 (1964) 1958.

88 V. Amirthalingam and K.V. Muralidharan, J. Inorg. Nucl. Chem., 26 (1964) 2038.

89 P.W. Wilson, Rev. Pure Appl. Chem., 22 (1972) 1.

90 R.C.L. Mooney, Acta Crystallogr., 2 (1949) 189.

91 K. Mucker, G.S. Smith, Q. Johnson and R.E. Elson, Acta Crystallogr., Sect. B, 25 (1969) 2362.

92 J.L. Hoard and J.V. Silverton, Inorg. Chem., 2 (1963) 235.

93 D. Brown, T.L. Hall and P.T. Moseley, J. Chem. Soc., Dalton Trans., (1973) 686.

94 P. Chiotti, G.J. Gartner, E.R. Stevens and Y. Saito, J. Chem. Eng. Data, 11 (1966) 571.

95 D.E. Scaife, Inorg. Chem., 5 (1966) 162.

96 R.M. Douglass and E. Staritzky, Anal. Chem., 29 (1957) 459.

97 A. Zalkin, J.D. Forrester and D.H. Templeton, Inorg. Chem., 3 (1964) 639.

98 G.D. Brunton, Acta Crystallogr., 21 (1964) 814.

99 G. Brunton, Acta Crystallogr., Sect. B, 25 (1969) 2163.

100 D. Brown, The Transuranium Elements, Gmelin 71, 1972, Chaps. 3.5—3.8.

101 L.A. Harris, Acta Crystallogr., 13 (1960) 502.

102 A. Rosenzweig and D.T. Cromer, Acta Crystallogr., Sect. B, 26 (1970) 38.

103 F.H. Kruse, J. Inorg. Nucl. Chem., 33 (1971) 1615.

104 G. Brunton, J. Inorg. Nucl. Chem., 29 (1967) 1631.

105 G. Brunton, Acta Crystallogr., Sect. B, 27 (1971) 2290.

106 J.H. Burns, R.D. Ellison and H.A. Levy, Acta Crystallogr., Sect. B, 24 (1968) 230.

107 R.A. Walton, Prog. Inorg. Chem., 16 (1972) 1.

108 B. Krebs, Angew. Chem. Int. Ed., 8 (1969) 146.

109 M. Elder and B.R. Penfold, Inorg. Chem., 5 (1966) 1197.

110 L.F. Dahl and D.L. Wampler, Acta Crystallogr., 15 (1962) 903.

111 F.A. Cotton, B.G. de Boer and Z. Mester, J. Am. Chem. Soc., 95 (1973) 1159.

112 G.S. Smith, Q. Johnson and R.E. Elson, Acta Crystallogr., 22 (1967) 300.

113 F. Lux, G. Wirth and K.W. Bagnall, Chem. Ber., 103 (1970) 2807.

114 R.P. Dodge, G.S. Smith, Q. Johnson and R.E. Elson, Acta Crystallogr., 22 (1967) 85.

115 D. Brown, T.J. Petcher and A.J. Smith, Acta Crystallogr., Sect. B, 25 (1969) 178.

116 A. Zalkin and D.E. Sands, Acta Crystallogr., 11 (1958) 615.

117 D.E. Sands and A. Zalkin, Acta Crystallogr., 12 (1959) 723.

118 K. Mucker, G.S. Smith and Q. Johnson, Acta Crystallogr., Sect. B, 24 (1968) 874.

119 S.M. Ohlberg, J. Am. Chem. Soc., 81 (1959) 811.

120 A.J. Edwards, J. Chem. Soc., (1964) 3714.

121 A.J. Edwards, R.D. Peacock and R.W.H. Small, J. Chem. Soc., (1962) 4486.

122 A.J. Edwards, J. Chem. Soc. A, (1969) 909.

123 A.J. Edwards and G.R. Jones, J. Chem. Soc., A, (1968) 2074.

124 A.J. Edwards and G.R. Jones, J. Chem. Soc., (1969) 1651.

125 A.J. Edwards, Proc. Chem. Soc., London, (1963) 205.

126 N. Bartlett and P.R. Rao, Chem. Commun., (1965) 252.

127 J.H. Holloway, R.D. Peacock and R.W.H. Small, J. Chem. Soc., (1964) 644.

128 A.J. Edwards and B.R. Steventon, J. Chem. Soc. A, (1968) 2503.

129 A.J. Edwards, G.R. Jones and B.R. Steventon, Chem. Commun., (1967) 462.

130 A.J. Edwards and G.R. Jones, J. Chem. Soc. A, (1968) 2511.

131 S.J. Mitchell and J.H. Holloway, J. Chem. Soc. A, (1971) 2789.

132 A.J. Edwards, G.R. Jones and R.J.C. Sills, Chem. Commun., (1968) 1177.

133 A.J. Edwards, W.E. Falconer and W.A. Sunder, J. Chem. Soc., Dalton Trans., (1974) 541.

134 R.T. Paine and L.B. Asprey, Inorg. Chem., 14 (1975) 1111.

135 B.K. Morrell, A. Zalkin, A. Tressaud and N. Bartlett, Inorg. Chem., 12 (1973) 2640.

136 J.G. Malm and B. Weinstock, Proc. 2nd Int. Conf. Peaceful Uses Atomic Energy, 28 (1958) 125.

137 A.E. Florin, I.A. Tannenbaum and J.F. Lemons, J. Inorg. Nucl. Chem., 2 (1956) 368.

138 P. Rigny and J. Virlet, J. Chem. Phys., 51 (1969) 3807.

139 D.W.J. Cruickshank, Acta Crystallogr., 9 (1956) 754.

140 S. Siegel and D.A. Northrop, Inorg. Chem., 5 (1966) 2187.

141 J.H. Levy, J.C. Taylor and P.W. Wilson, Acta Crystallogr., Sect. B, 31 (1975) 398.

142 J.H. Levy, J.C. Taylor and P.W. Wilson, J. Solid State Chem., 15 (1975) 360.

143 R. Blinc and G. Lahajnar, Phys. Rev. Lett., 19 (1967) 685.

144 P. Rigny, M. Drifford and J. Virlet, J. Phys., 32 (1971) C5a—229.

145 J. Virlet and P. Rigny, Chem. Phys. Lett., 6 (1970) 377.

146 J. Michel, M. Drifford and P. Rigny, J. Chim. Phys., 67 (1970) 31.

147 J.C. Taylor and A.B. Waugh, J. Solid State Chem., (1976) in press.

148 F.C. von der Lage and H.A. Bethe, Phys. Rev., 71 (1947) 612.

149 J. Gaunt, Trans. Faraday Soc., 50 (1954) 546.

150 M. Kimura, V. Schomaker, D.W. Smith and B. Weinstock, J. Chem. Phys., 48 (1968) 4001.

151 V.C. Ewing and L.E. Sutton, Trans. Faraday Soc., 59 (1963) 1241.

152 T.A. O'Donnell, D.F. Stewart and P. Wilson, Inorg. Chem., 5 (1966) 1438.

153 W.H. Zachariasen, Acta Crystallogr., 1 (1948) 285.

154 J.A.A. Ketelaar and G.W. van Oosterhout, Rec. Trav. Chim. Pays-Bas, 62 (1943) 197.

155 J.H. Canterford and R. Colton, Halides of the Second and Third Row Transition Metals, Wiley, New York, 1968.

156 W.H. Zachariasen, Acta Crystallogr., 4 (1951) 231.

157 A.W. Mann and D.J.M. Bevan, Acta Crystallogr., Sect. B, 26 (1970) 2129.

158 B. Holmberg, Acta Chem. Scand., 20 (1966) 1082.

159 R.C. Garvie in A.M. Alper (Ed.), High Temperature Oxides, Academic Press, New York, 1970, Chap. 4.

160 D.J.M. Bevan and A.W. Mann, Acta Crystallogr., Sect. B, 31 (1975) 1406.

161 N. Rysanek and O. Loye, Acta Crystallogr., Sect. B, 29 (1973) 1567.

162 Nguyen Huy - Dung, Acta Crystallogr., Sect. B, 29 (1973) 2095.

163 N. Savigny, P. Laruelle and J. Flahaut, Acta Crystallogr., Sect. B, 29 (1973) 345.

164 N. Savigny, C. Adolphe, A. Zalkin and D.H. Templeton, Acta Crystallogr., Sect. B, 29 (1973) 1532.

165 R.P. Dodge, G.S. Smith, Q. Johnson and R.E. Elson, Acta Crystallogr., Sect. B, 24 (1968) 304.

166 K.W. Bagnall, D. Brown and J.F. Easey, J. Chem. Soc. A., (1968) 288.

167 D.E. Scaife, A.G. Turnbull and A.W. Wylie, J. Chem. Soc., (1965) 1432.

168 D. Brown and P.J. Jones, J. Chem. Soc. A, (1967) 719.

169 D. Brown, T.J. Petcher and A.J. Smith, Nature (London), 217 (1968) 737.

170 D. Brown, T.J. Petcher and A.J. Smith, Acta Crystallogr., Sect. B, 31 (1975) 1382.

171 J.G. Allpress and A.D. Wadsley, Acta Crystallogr., 17 (1964) 41.

172 J. Levet, C.R. Acad. Sci., 268 (1969) 703.

173 W.H. Zachariasen, Acta Crystallogr., 1 (1948) 277.

174 J.C. Taylor and P.W. Wilson, Aust. A.E.C., AAEC/E255 (Rep.), (1973).

175 M. Atoji and M.J. McDermott, Acta Crystallogr., Sect. B, 26 (1970) 1540.

176 K.W. Bagnall, D. Brown and J.F. Easey, J. Chem. Soc. A, (1968) 2223.

177 I.F. Alenchickova, L.L. Zaitseva, L.V. Lipis, N.S. Nikolaev, V.V. Fomin and N.T. Chebotarev, Zh. Neorg. Khim., 3 (1958) 951.

178 T.K. Keenan, Inorg. Nucl. Chem. Lett., 4 (1968) 381.

179 W.H. Zachariasen, Acta Crystallogr., 7 (1954) 792.

180 N. Quy- Dao, H. Brusset and A. Rubinstein-Auban, J. Inorg. Nucl. Chem., 34 (1972) 1575.

181 H. Brusset, H. Gillier-Pandraud and N. Quy-Dao, Acta Crystallogr., Sect. B, 25 (1969) 67.

182 H. Brusset, N. Quy-Dao and A. Rubinstein-Auban, Acta Crystallogr., Sect. B, 28 (1972) 2617.

183 N. Quy-Dao, Acta Crystallogr., Sect. B, 28 (1972) 2011.

184 H. Brusset, N. Quy-Dao and S. Chourou, Acta Crystallogr., Sect. B, 30 (1974) 768.

185 V.G. Kuznetsov et al., Zh. Strukt. Khim., 15 (1974) 943.

186 Y.N. Mikhailov, A.A. Vdovenko, V.G. Kuznetsov and R.L. Davidovich, Zh. Strukt. Khim., 13 (1972) 942.

187 J.H. Levy, J.C. Taylor and P.W. Wilson, J. Inorg. Nucl. Chem., (1976) to be submitted.

188 I.R. Beattie and D.J. Reynolds, Chem. Commun., (1968) 1531.

189 P.W. Wilson, J. Inorg. Nucl. Chem., 36 (1974) 1783.

190 G. Fonteneau, H. L'Helgoualch and J. Lucas, Inorg. Nucl. Chem. Lett., 11 (1975) 297.

191 P.C. Debets, Acta Crystallogr., Sect. B, 24 (1968) 400.

192 M. Aberg, Acta Chem. Scand., 23 (1969) 791.

193 M. Aberg, Acta Chem. Scand., 25 (1971) 368.

194 M.G.B. Drew and I.B. Tomkins, J. Chem. Soc. A, (1970) 22.

195 G. Ferguson, M. Mercer and D.W.A. Sharp, J. Chem. Soc. A, (1969) 2415.

196 D.E. Sands, A. Zalkin and R.E. Elson, Acta Crystallogr., 12 (1959) 21.

197 C.G. Barraclough and J. Stals, Aust. J. Chem., 19 (1966) 741.

198 O. Jarchow, F. Schroder and H. Schulz, Z. Anorg. allg. Chem., 363 (1968) 58.

199 L.O. Atovmyan, Z.G. Aliev and B.M. Tarakanov, J. Struct. Chem. (U.S.S.R.), 9 (1968) 985.
200 J. Tillack and P. Eckerlin, Angew. Chem., Int. Ed. Eng., 5 (1966) 421.
201 L.O. Atovmyan and Z.G. Aliev, J. Struct. Chem. (U.S.S.R.), 12 (1971) 668.
202 A.J. Edwards and P. Taylor, Chem. Commun., (1970) 1474.
203 A.J. Edwards, J. Chem. Soc., Dalton Trans., (1972) 582.
204 P.W. Frais and C.J.L. Lock, Can. J. Chem., 50 (1972) 1811.
205 H.O. Haug and R.D. Baybarz, Inorg. Nucl. Chem. Lett., 11 (1975) 847.